Spline-based frames in the space of periodic signals

Amir Averbuch[1] Pekka Neittaanmäki[2] Valery Zheludev[1]
[1]School of Computer Science
Tel Aviv University, Tel Aviv 69978, Israel

[2]Department of Mathematical Information Technology
P.O. Box 35 (Agora), University of Jyväskylä, Finland

Abstract

We present a design scheme to generate tight and semi-tight frames in the space of discrete-time periodic signals, which are originated from four-channel perfect reconstruction periodic filter banks. The filter banks are derived from interpolating and quasi-interpolating polynomial splines. Each filter bank comprises one linear phase low-pass filter (in most cases interpolating) and one high-pass filter, whose magnitude's response mirrors that of a low-pass filter. In addition, these filter banks comprise two band-pass filters. In the semi-tight frames case, all the filters have linear phase and (anti)symmetric impulse response, while in the tight frame case, some of band-pass filters are slightly asymmetric. We introduce the notion of local discrete vanishing moments (LDVM). In the tight frame case, analysis framelets coincide with their synthesis counterparts. However, in the semi-tight frames, we have the option to swap LDVM between synthesis and analysis framelets. The design scheme is generic and it enables us to design framelets with any number of LDVM. The computational complexity of the framelet transforms, which consists of calculation of the forward and the inverse fast Fourier transforms and simple arithmetic operations, practically does not depend on the number of LDVM and does depend on the size of the impulse response of filters . The designed frames are used for image restoration tasks, which are degraded by blurring, random noise and missing pixels. The images were restored by the application of the Split Bregman Iterations method. The frame performances are evaluated.

1 Introduction

Restoration of corrupted and/or damaged and/or noised multidimensional signals is a major challenge that the signal/image processing community faces nowadays when rich multimedia content is the most popular data that is being transmitted over diverse networks types such as mobile. Quality degradation in multidimensional signals can come from sampling, acquisition, transmission through noisy channels, to name some. Restoration of multidimensional signals includes denoising, deblurring, recovering missing or damaged samples or fragments (inpainting in images), resolution enhancement and super resolution. The processing goals are to improve the visual perception of still and video signals. But no less important are the goals to reveal internal fine structures and details in these multidimensional signals by extracting characteristic objects features or classes of objects.

Recent developments in wavelet frames (framelets) analysis provide innovative and powerful tools to process faithfully and robustly the above challenges. Framelets produce redundant expansions for multidimensional signals that, in particular, provide an additional sparsity to the signals representation due to better adaptation abilities of redundant representations. A valuable advantage that redundant representations hold is their ability to restore missing and incomplete information and to represent efficiently and compactly the data.

Frame expansions of signals demonstrate resilience to the coefficients disturbances and losses [18, 17, 22, 1]. Thus, frames can serve as a tool for error correction for signals transmitted through lossy channels.

Implicitly, this resilience is utilized in signal/image restoration, which is based on the prior assumption that a frame expansion of a given signal/image is sparse. In principle, only part of the samples/pixels is needed to (near) perfect object restoration. This approach, which is a variation of the *Compressive Sensing* methodology ([15], for example), proved to be extremely efficient for image restoration.

Practically, this approach is implemented via minimization of a parameterized functional where the sparse representation is reflected in the l_1 norm of the transform coefficients. The $\|\cdot\|_1$ minimization does not have an explicit solution and can be resolved only by iterative methods. The so-called *split Bregman iteration* (SBI) scheme, which was recently introduced in [16], provided a fast and stable algorithm for that. Variations of this scheme and its application to image restoration using wavelet frames are described in [21, 20], to mention a few. A variety of impressive results on image restoration were reported in the last couple of years. A survey is given in [26] while a recent development is described in [20].

Due to applications diversity, it is important to have a library of wavelet frames in order to select a frame that fits best a specific task. Forward and inverse transforms in iterative algorithms are repeated many times, therefore, members in this library must have fast and stable transforms implementation. Waveforms symmetry with the availability of vanishing moments are also important in order to avoid distortions when thresholding is used. To satisfy these requirements, most of the framelet systems that were designed so far operate with the compactly supported framelets and the transforms are implemented by finite (and short) impulse response (FIR) oversampled filter banks [14, 11, 12, 9]. Thus, the number of framelet systems available for applications is very limited. This number is even smaller when the requirement is to have tight frames.

The oversampled perfect reconstruction (PR) filter banks generate wavelet-type frames in the space of discrete-time signals [13, 10]. Utilizing infinite impulse response (IIR) filter banks with a relaxation of the tightness requirement provides a number of additional opportunities. Properties such as symmetry, interpolation, flat spectra combined with fine time-domain localization of framelets can be easily achieved as well as a high number of vanishing moments [7, 6]. In these papers, the key point is the low-pass filters design, which, being applied to the even subarray of a signal, well approximate the odd subarray (the prediction filters). A natural source for such filters are the discrete and polynomial splines. A number of 3-framelet systems was derived from the discrete splines in [7, 6]. The transforms are implemented in a fast way using recursive filtering. Non-compactness of the waveforms supports is compensated by their exponential decay as time goes to infinity. In principle, any number of vanishing moments can be derived but the implementation computational cost grows fast.

This drawback can be overcome by switching to a periodic setting, which is the subject of this paper. A variety of four-channel PR filter banks, where the low-pass filters are derived from interpolating and quasi-interpolating polynomial splines, are designed. These filter banks generate a library of 4- framelet periodic tight and the so-called semi-tight frames with diverse properties. The transforms implementation is reduced to application of the direct and the inverse fast Fourier transforms (FFT) with simple arithmetic operations. Altogether, 18 framelets systems are explicitly designed and described in this paper. However, the design scheme is generic and this framelets library can be easily expanded. Preliminary results in the periodic discrete-time frame design with three framelets are reported in [28]. Recently, framelets in the space of periodic continuous functions were studied in [24].

The designed framelets libraries were tested for image restoration and demonstrated a high quality. Their diversity enabled us to select a frame, which best fits each specific application. In particular, in most of the experiments the semi-tight frames outperformed tight frames.

The paper is organized as follows. The introductory section 2 recalls the notions of periodic discrete-time signals and of periodic filter (p-filter). In section 3, the PR periodic filter banks (p-filter banks) are presented and characterized via the polyphase representation of their discrete Fourier transform (DFT). Section 4 introduces frames in the discrete-time periodic signals space, which originated from PR oversampled p-filter banks. Design of four-channel p-filter banks, which generate tight and semi-tight frames, is presented in section 5. Section 6 discusses the restoration of sampled polynomials by low-pass p-filters and introduces the notion of local discrete vanishing moments (LDVM). A collection of FIR and IIR p-filters is derived in section 7 from the interpolating and quasi-interpolating splines. A number of four-channel p-filter banks

with spline p-filters that generate tight and semi-tight frames is described in section 8. The designed tight and semi-tight frames are used in section 9 for image restoration, which were degraded by blurring, random noise and missing pixels. The frames performances are evaluated.

2 Periodic discrete-time signals and filters

2.1 Signals and transforms

We call the N-periodic real-valued sequences $\mathbf{x} \stackrel{\text{def}}{=} \{x[k]\},\ k \in \mathbb{Z},\ x[k+N] = x[k]$, the discrete-time periodic signals. In the sequel, we assume that $N = 2^j$, j is a natural number and $\omega \stackrel{\text{def}}{=} e^{2\pi i/N}$. These signals form an N-dimensional vector space, which we denote by $\Pi[N]$, where the inner product and the norm are defined as $\langle \mathbf{x}, \mathbf{h} \rangle \stackrel{\text{def}}{=} \sum_{k=0}^{N-1} x[k]\, h[k], \quad \|\mathbf{x}\| = \|\mathbf{x}\|_2 \stackrel{\text{def}}{=} \sqrt{\sum_{k=0}^{N-1} |x[k]|^2}$, respectively.

Note that any discrete-time signal $\mathbf{y}$ of limited duration L can be embedded into a space $\Pi[N],\ N \geq L$, by the periodization $\tilde{\mathbf{y}} \stackrel{\text{def}}{=} \left\{\tilde{y}[k] = \sum_{l \in \mathbb{Z}} y[k + lN]\right\}$.

The discrete circular convolution of two N-periodic signals is an N-periodic signal$\mathbf{y} = \mathbf{h} \circledast \mathbf{x} \Longleftrightarrow y[k] = \sum_{l=0}^{N-1} h[k-l]\, x[l]$. The discrete Fourier transform (DFT) of a signal $\mathbf{x}$ and its inverse (IDFT) are $\hat{x}[n] = \sum_{k=0}^{N-1} x[k]\, \omega^{-nk}$ and $x[k] = 1/N \sum_{n=0}^{N-1} \hat{x}[n]\, \omega^{nk}$, respectively. Both the DFT and the IDFT are calculated by the fast Fourier transform (FFT) algorithm Since the signals are real-valued, the complex conjugate DFT becomes $\hat{x}[n]^* = \hat{x}[-n]$.

We use the notations $\hat{x}[n]_m = \sum_{k=0}^{N/2^m-1} x[k]\, \omega^{-2^m nk}$, $x[k] = 2^m/N \sum_{n=0}^{N/2^m-1} \hat{x}[n]_m\, \omega^{2^m nk}$ *for the DFT of signals belonging to the space* $\Pi[N/2^m]$. *The sequence* $\{\hat{x}[n]_m\}$ *is* $N/2^m$*-periodic.*
The following relations between signals from $\Pi[N]$ and their DFT hold:

Parseval identities: $\langle \mathbf{x}, \mathbf{h} \rangle = 1/N \sum_{n=-N/2}^{N/2-1} \hat{x}[n]\, \hat{h}[-n], \quad \|\mathbf{x}\|^2 = 1/N \sum_{n=-N/2}^{N/2-1} |\hat{x}[n]|^2$.

Circular convolution: If $\mathbf{y} = \mathbf{x} \circledast \mathbf{h}$ then $\hat{y}[n] = \hat{h}[n]\, \hat{x}[n]$.

Circular shift: If $\mathbf{x}_d \stackrel{\text{def}}{=} \{x[k+d]\}$, where d is an integer number, then $\hat{x}_d[n] = \omega^{nd}\, \hat{x}[n]$.

Finite differences: The finite differences of a sequence $\mathbf{x}$ are defined iteratively:
$\Delta[\mathbf{x}] \stackrel{\text{def}}{=} \{x[k+1] - x[k]\},\ k \in \mathbb{Z},\ \Delta^n[\mathbf{x}] \stackrel{\text{def}}{=} \Delta[\Delta^{n-1}[\mathbf{x}]]$. The central finite difference of second order $\delta^2[\mathbf{x}] \stackrel{\text{def}}{=} \{x[k+1] - 2x[k] + x[k-1]\},\ k \in \mathbb{Z}$, and $\delta^{2r}[\mathbf{x}] \stackrel{\text{def}}{=} \delta^2[\delta^{2n-2}[\mathbf{x}]]$.

Proposition 2.1 *Assume that* $\mathbf{P_{n-1}} \stackrel{\text{def}}{=} \{P_{n-1}(k)\},\ k \in \mathbb{Z}$, *is a sampled polynomial of degree not exceeding* $n-1$. *Then,* $\Delta^n[\mathbf{P_{n-1}}] = \mathbf{0}$. *If* $n = 2r$ *then* $\delta^{2r}[\mathbf{P_{2r-1}}] = \mathbf{0}$.

If $\mathbf{x} \in \Pi[N]$ then their differences belong to $\Pi[N]$ and their DFTs are

$$\hat{\Delta}^m[\mathbf{x}][n] = (\omega^n - 1)^m\, \hat{x}[n], \quad \hat{\delta}^{2l}[\mathbf{x}][n] = \left(2i \sin \frac{\pi n}{N}\right)^{2l} \hat{x}[n]. \tag{2.1}$$

Polyphase representation of the DFT The signals $\mathbf{x}_0 = \{x[2k]\}$ and $\mathbf{x}_1 = \{x[2k+1]\}$ belonging to $\Pi[N/2]$ are called the even and the odd polyphase components of the signal $\mathbf{x} \in \Pi[N]$, respectively.

Their DFTs are

$$\begin{aligned} &\hat{x}[n] = \hat{x}_{0,2}[n]_1 + \omega^{-n}\, \hat{x}_{1,2}[n]_1, \quad \hat{x}[n+N/2] = \hat{x}_{0,2}[n]_1 - \omega^{-n}\, \hat{x}_{1,2}[n]_1 \\ &\Longrightarrow \hat{x}_{0,2}[n]_1 = (\hat{x}[n] + \hat{x}[n+N/2])/2, \quad \hat{x}_{1,2}[n]_1 = (\hat{x}[n] - \hat{x}[n+N/2])/2\omega^{-n}. \end{aligned} \tag{2.2}$$

2.2 Periodic filters

A linear operator of $\mathbf{h} : \Pi[N] \longrightarrow \Pi[N], \quad \mathbf{y} = \mathbf{h}\mathbf{x}$, is time-invariant if the shift $\mathbf{x}_d \stackrel{\text{def}}{=} \{x[k+d]\}$ of the input signal produces the same output for the shift $\mathbf{y}_d \stackrel{\text{def}}{=} \{y[k+d]\}$. Such operators are called digital periodic filters (p-filters). Application of the p-filter to a periodic signal is implemented via the discrete circular convolution $\mathbf{y} = \mathbf{h}\,\mathbf{x} = \mathbf{h} \circledast \mathbf{x} \Longleftrightarrow y[k] = \sum_{l=0}^{N-1} h[k-l]\,x[l]$.

The signal $\mathbf{h} = \{h[k]\} \in \Pi[N]$ is called the *impulse response* (IR) of the p-filter $\mathbf{h}$. We use the notation $\mathbf{h}$ for both a p-filter and its IR $\{h[k]\}$. The DFT of the IR of the p-filter $\mathbf{h}$ is $\hat{h}[n] = \sum_{l=0}^{N-1} h[k]\,\omega^{-nk}, \quad n \in \mathbb{Z}$ and it is called a frequency response (FR).

Periodic filtering of a signal reduces to multiplication in the frequency domain: $\mathbf{h} \circledast \mathbf{x} \Longleftrightarrow \hat{h}[n]\,\hat{x}[n], \quad n \in \mathbb{Z}$. The FR of a p-filter can be represented in a polar form $\hat{h}[n] = \left|\hat{h}[n]\right| e^{i\,\arg(\hat{h}[n])}$, where the positive N-periodic sequence $\left|\hat{h}[n]\right|$ is called the magnitude response (MR) of $\mathbf{h}$ and the real-valued 2π-periodic sequence $\arg(\hat{h}[n])$ is called the phase response of $\mathbf{h}$. A p-filter is referred to as a linear phase if its phase response is linear in n. If the IR of a filter $\mathbf{h}$ is symmetric or antisymmetric within the interval $k = -N/2, ..., N/2-1$, then $\mathbf{h}$ is a linear phase filter.

3 Periodic filter banks

3.1 Multirate p-filtering

Assume that $\mathbf{x} \stackrel{\text{def}}{=} \{x[k]\}$ belongs to $\Pi[N]$, $N = 2^j$, and $M = 2^l$, $l < j$. The operation $(\downarrow M)\mathbf{x} = \grave{\mathbf{x}} \stackrel{\text{def}}{=} \{x[Mk]\} \in \Pi[N/M]$ is called downsampling the signal $\mathbf{x}$ by factor of M. Assume that a signal $\mathbf{x}$ belongs to $\Pi[N/M]$. The operation

$$(\uparrow M)\mathbf{x} = \acute{\mathbf{x}}, \quad \acute{x}[k] = \begin{cases} x[l], & \text{if } k = lM; \\ 0, & \text{otherwise.} \end{cases}, \quad l \in \mathbb{Z},$$

is called upsampling the signal $\mathbf{x}$ by factor of M. In the rest of the paper, we assume that the down(up)sampling factor ia $M = 2$. Then, the downsampled signal $(\downarrow 2)\mathbf{x} = \mathbf{x}_0$ is the evenpolyphase component of the signal $\mathbf{x}$, while the upnsampled signal $(\uparrow 2)\mathbf{x}$ is a signal, whose odd polyphase component vanishes.

If p-filtering of a signal is accompanied by downsampling or upsampling then it is called multirate p-filtering. Let $\mathbf{h} = \{h[k]\}$ and $\tilde{\mathbf{h}} = \left\{\tilde{h}[k]\right\}$ be p-filters. Application of the p-filter $\bar{\mathbf{h}} = \left\{\tilde{h}[-k]\right\}$, which is the time-reversed filter $\tilde{\mathbf{h}}$, to the signal $\mathbf{x}$, which is followed by downsampling by factor of 2, produces the signal $\tilde{\mathbf{y}} = \{\tilde{y}[k]\} \in \Pi[N/2]$,

$$\tilde{y}[k] = \sum_{l=0}^{N-1} \tilde{h}[l-2k]\,x[l], \quad \widehat{\tilde{y}}[n] = \hat{\tilde{h}}_0[-n]_1\,\hat{x}_0[n]_1 + \hat{\tilde{h}}_1[-n]_1\,\hat{x}_1[n]_1, \quad n \in \mathbb{Z}. \tag{3.1}$$

Application of the p-filter $\mathbf{h}$ to a signal $\breve{\mathbf{y}} = \{\breve{y}[k]\} \in \Pi[N/2]$, which is upsampled by factor of 2, produces the signal $\breve{\mathbf{x}} = \{\breve{x}[k]\} \in \Pi[N]$,

$$\breve{x}[k] = \sum_{l=0}^{N/2-1} h[k-2l]\,\breve{y}[l], \quad \hat{\breve{x}}[n] = \hat{h}[n]\,\hat{\breve{y}}[n]_1 \Longrightarrow \hat{\breve{x}}_0[n]_1 = \hat{h}_0[n]_1\,\hat{\breve{y}}[n]_1, \quad \widehat{\breve{x}_1}[n]_1 = \hat{h}_1[n]_1\,\hat{\breve{y}}[n]_1. \tag{3.2}$$

Interpolating p-filters: If the DFT of the even polyphase component of a p-filter $\mathbf{h}$ is constant i.e. $\hat{h}_0[n]_1 \equiv C$ then the p-filter is called interpolating. In this case, Eq. (3.2) implies that the DFT of the zero polyphase component of the output signal is $\breve{\mathbf{x}}\ \hat{\breve{x}}_0[n]_1 = C\hat{\breve{y}}[n]_1$. This means that $\breve{x}[2k] = C\breve{y}[k],\ k \in \mathbb{Z}$.

3.2 Filter banks

The set of p-filters $\tilde{\mathbf{H}} \stackrel{\text{def}}{=} \left\{\tilde{\mathbf{h}}^s\right\}$, $s = 0, ..., S-1$, which, being time-reversed and applied to an input signal $\mathbf{x} \in \Pi[N]$, produces the set of the output signals $\{\tilde{\mathbf{y}}^s\}_{s=0}^{S-1}$ downsampled by factor of M,

$$\widetilde{y^s}[l] = \sum_{k=0}^{N-1} \tilde{h}^s[k - Ml]\, x[k], \quad s = 0, \ldots, S-1,\ l \in \mathbb{Z}. \tag{3.3}$$

It is called the $S-$channel analysis p-filter bank. The set of filters $\mathbf{H} \stackrel{\text{def}}{=} \{\mathbf{h}^s\}$, $s = 0, ..., S-1$, which, being applied to a set of input signals $\{\mathbf{y}^s\} \in \Pi[N/M]$, $s = 0, ..., S-1$, that are upsampled by factor of M, produces the output signal $\breve{x}[l]) = \sum_{s=0}^{S-1} \sum_{k=0}^{N/M-1} h^s[l - Mk]\, y^s[k]$, $l \in \mathbb{Z}$, is called the $S-$channel synthesis p-filter bank. If the upsampled signals $\tilde{\mathbf{y}}^{\mathbf{s}}$, $s = 0, \ldots, S-1$, which are defined in Eq. (3.3), are used as an input to the synthesis p-filter bank and the output signal is $\breve{\mathbf{x}} = \mathbf{x}$, then the pair of analysis–synthesis p-filter banks form a PR p-filter bank.

If the number of channels S equals to the downsampling factor M then the p-filter bank is said to be critically sampled. If $S > M$ then the p-filter bank is oversampled. Critically sampled PR p-filter banks are used in the wavelet analysis, while oversampled PR p-filter banks serve as a source for discrete-time wavelet frames design.

In the paper, we deal with p-filter banks, whose downsampling factor is $M = 2$ and $\tilde{\mathbf{h}}^0$ and $\mathbf{h}^0$ are the low-pass filters.

3.3 Characterization of p-filter banks

Assume that $\tilde{\mathbf{H}} \stackrel{\text{def}}{=} \left\{\tilde{\mathbf{h}}^s\right\}$, $s = 0, ..., S-1$, is an analysis p-filter bank with the downsampling factor of 2. Then, its application to a signal $\mathbf{x} \in \Pi[N]$ produces S signals from $\Pi[N/2]$:

$$\tilde{y}^s[l] = \sum_{k=0}^{N-1} \tilde{h}^s[k - 2l]\, x[k], \quad s = 0, \ldots, S-1,\ l \in \mathbb{Z}, \tag{3.4}$$

$$\hat{\tilde{y}}^s[n]_1 = \hat{\tilde{h}}_0^s[-n]_1\, \hat{x}_0[n]_1 + \hat{\tilde{h}}_1^s[-n]_1\, \hat{x}_1[n]_1, \quad n \in \mathbb{Z}. \tag{3.5}$$

Assume that $\mathbf{H} \stackrel{\text{def}}{=} \{\mathbf{h}^s\}$, $s = 0, ..., S-1$, is a synthesis p-filter bank with the upsampling factor of 2. Then, its application to the upsampled signals $\tilde{\mathbf{y}}^s \in \Pi[N/2]$ produces a signal from $\Pi[N]$:

$$\breve{x}[l] = \sum_{s=0}^{S-1} \sum_{k=0}^{N/2-1} h^s[l - 2k]\, \tilde{y}^s[k], \quad l \in \mathbb{Z}, \tag{3.6}$$

$$\hat{\breve{x}}_0[n]_1 = \sum_{s=0}^{S-1} \hat{h}_0^s[n]_1\, \hat{\tilde{y}}^s[n]_1, \quad \hat{\breve{x}}_1[n]_1 = \sum_{s=0}^{S-1} \hat{h}_1^s[n]_1\, \hat{\tilde{y}}^s[n]_1. \tag{3.7}$$

Equations (3.5) and (3.7) can be written in a matrix form by

$$\begin{pmatrix} \hat{\tilde{y}}^0[n]_1 \\ \vdots \\ \hat{\tilde{y}}^{S-1}[n]_1 \end{pmatrix} = \tilde{\mathbf{P}}[-n] \cdot \begin{pmatrix} \hat{x}_0[n]_1 \\ \hat{x}_1[n]_1 \end{pmatrix}, \quad \begin{pmatrix} \hat{\breve{x}}_0[n]_1 \\ \hat{\breve{x}}_1[n]_1 \end{pmatrix} = \mathbf{P}[n] \cdot \begin{pmatrix} \hat{\tilde{y}}^0[n]_1 \\ \vdots \\ \hat{\tilde{y}}^{S-1}[n]_1 \end{pmatrix}$$

where the $S \times 2$ analysis and the $2 \times S$ synthesis polyphase matrices are, respectively,

$$\tilde{\mathbf{P}}[n] \stackrel{\text{def}}{=} \begin{pmatrix} \hat{\tilde{h}}_0^0[n]_1 & \hat{\tilde{h}}_1^0[n]_1 \\ \vdots & \vdots \\ \hat{\tilde{h}}_0^{S-1}[n]_1 & \hat{\tilde{h}}_1^{S-1}[n]_1 \end{pmatrix} \quad \mathbf{P}[n] \stackrel{\text{def}}{=} \begin{pmatrix} \hat{h}_0^0[n]_1 & \ldots & \hat{h}_0^{S-1}[n]_1 \\ \hat{h}_1^0[n]_1 & \ldots & \hat{h}_1^{S-1}[n]_1 \end{pmatrix}, \quad n \in \mathbb{Z}.$$

If the relations

$$\mathbf{P}[n] \cdot \tilde{\mathbf{P}}[-n] = \mathbf{I}_2, \tag{3.8}$$

hold for all $n \in \mathbb{Z}$ when $\mathbf{I}_2$ is the 2×2 identity matrix, then

$$\mathbf{P}[n] \cdot \tilde{\mathbf{P}}[-n] \cdot \begin{pmatrix} \hat{x}_0[n]_1 \\ \hat{x}_1[n]_1 \end{pmatrix} = \begin{pmatrix} \hat{x}_0[n]_1 \\ \hat{x}_1[n]_1 \end{pmatrix}.$$

Thus, Eq. (3.8) is the condition for the pair $\left\{\tilde{\mathbf{H}},\, \mathbf{H}\right\}$ of p-filter banks to form a PR p-filter bank.

4 Frames in the periodic signals space

Definition 4.1 *A system $\tilde{\Phi} \stackrel{\text{def}}{=} \{\tilde{\phi}_l\}_{l=0}^{L-1}$, $L \geq N$, of signals from $\Pi[N]$ forms a frame for the space $\Pi[N]$ if there exist positive constants A and B such that for any signal $\mathbf{x} = \{x[k]\} \in \Pi[N]$ we have $A\|\mathbf{x}\|^2 \leq \sum_{l=0}^{L-1} |\langle \mathbf{x}, \tilde{\phi}_l \rangle|^2 \leq B\|\mathbf{x}\|^2$. If the frame bounds A and B are equal to each other then the frame is said to be tight.*

If the system $\tilde{\Phi}$ is a frame then there exists another frame $\Phi \stackrel{\text{def}}{=} \{\phi_l\}_{l=0}^{L-1}$ in the space $\Pi[N]$ such that any signal $\mathbf{x} \in \Pi[N]$ can be expanded into the sum $\mathbf{x} = \sum_{l=0}^{L-1} \langle \mathbf{x}, \tilde{\phi}_l \rangle\, \phi_l$. The analysis $\tilde{\Phi}$ and the synthesis Φ frames can be interchanged. Together they form the so-called bi-frame. If the frame is tight then Φ can be chosen as $\Phi = c\tilde{\Phi}$.

If the elements $\{\tilde{\phi}_l\}$ of the analysis frame $\tilde{\Phi}$ are not linearly independent ($L > N$) then many synthesis frames can be associated with a given analysis frame. In this case, the expansions $\mathbf{x} = \sum_{l=0}^{L-1} \langle \mathbf{x}, \tilde{\phi}_l \rangle\, \phi_l$ provide redundant representations of the signal $\mathbf{x}$.

It was established in [13] that the PR filter banks operating in the space l_1 of decaying discrete-time signals generate frames for this space. A similar fact was proved in [28] for the p-filter banks operating in $\Pi[N]$.

4.1 Wavelet frame transform

Assume an analysis $\tilde{\mathbf{H}} \stackrel{\text{def}}{=} \left\{\widetilde{\mathbf{h}^s}\right\}$, $s = 0, ..., S-1$, and a synthesis $\mathbf{H} \stackrel{\text{def}}{=} \{\mathbf{h}^s\}$, $s = 0, ..., S-1$, p-filter banks with downsampling by factor of 2 form a PR p-filter bank.

Denote

$$\tilde{\psi}^s_{[1]} \stackrel{\text{def}}{=} \left\{\tilde{\psi}^s_{[1]}[l] = \tilde{h}^s[l]\right\}_{l=0}^{N-1}, \quad \psi^s_{[1]} \stackrel{\text{def}}{=} \left\{\psi^s_{[1]}[l] = h^s[l]\right\}_{l=0}^{N-1},\ s = 0, ..., S-1, \tag{4.1}$$

where $\left\{\tilde{h}^s[l]\right\}$ and $\{h^s[l]\}$ are the impulse responses of the p-filters $\tilde{\mathbf{h}}^s$ and $\mathbf{h}^s$, respectively. Then, Eqs. (3.4) and (3.6) imply that $x[k] = \sum_{s=0}^{S-1} x^s_{[1]}[k]$, where

$$x^s_{[1]}[k] \stackrel{\text{def}}{=} \sum_{l=0}^{N/2-1} y^s_{[1]}[l]\, \psi^s_{[1]}[k-2l], \quad y^s_{[1]}[l] = \sum_{\kappa=0}^{N-1} \tilde{\psi}^s_{[1]}[\kappa - 2l]\, x[\kappa] = \langle \mathbf{x}, \tilde{\psi}^s_{[1]}[\cdot - 2l] \rangle, \tag{4.2}$$

$$\Longleftrightarrow \mathbf{x} = \sum_{s=0}^{S-1} \mathbf{x}^s_{[1]} = \sum_{s=0}^{S-1} \sum_{l=0}^{N/2-1} \langle \mathbf{x}, \tilde{\psi}^s_{[1]}[\cdot - 2l] \rangle\, \psi^s_{[1]}[\cdot - 2l]. \tag{4.3}$$

Thus, the signal $\mathbf{x} \in \Pi[N]$ is expanded over the system $\left\{\psi^s_{[1]}[\cdot - 2l]\right\}$, $s = 0, ..., S-1$, $l = 0, ..., \frac{N}{2} - 1$. The expansion coefficients are the inner products $\left\{\langle \mathbf{x}, \tilde{\psi}^s_{[1]}[\cdot - 2l] \rangle\right\}$.

Theorem 4.2 ([28]) *If the polyphase matrices* $\tilde{\mathbf{P}}$ *and* $\mathbf{P}$ *of the p-filter banks* $\tilde{\mathbf{H}}$ *and* $\mathbf{H}$ *satisfy the PR conditions Eq. (3.8), then the 2-sample circular shifts* $\left\{\tilde{\psi}^s_{[1]}[\cdot - 2l]\right\}$ *and* $\left\{\psi^s_{[1]}[\cdot - 2l]\right\}$, $s = 0, ..., S-1$, $l = 0, ..., N/2-1$ *of the signals* $\tilde{\psi}^s_{[1]}$ *and* $\psi^s_{[1]}$, $s = 0, ..., S-1$, *defined in Eq. (4.1), form a bi-frame of the space* $\Pi[N]$, *respectively. If the relations*

$$\tilde{\mathbf{P}}[n]^T \cdot \tilde{\mathbf{P}}[-n] = c\mathbf{I}_2, \quad n \in \mathbb{Z}, \tag{4.4}$$

hold then the frame is tight.

The notation $\cdot^T$ means matrix transposition. If the condition in Eq. (4.4) is satisfied, then the synthesis filter bank can be chosen to be equal to the analysis filter banl (up to a constant factor).

If $S > 2$ then the representation in Eq. (4.3) of a signal from $\Pi[N]$ is redundant. The redundancy ratio for one-level frame transform is $\rho = S/2$.

The signals $\tilde{\psi}^s_{[1]}$ and $\psi^s_{[1]}$, $s = 0, ..., S-1$, are called the analysis and synthesis discrete-time *framelets* of the first decomposition level, respectively.

4.2 Multi-level frame transform

Assume that the analysis $\tilde{\mathbf{H}}_{[\mu]} \stackrel{\text{def}}{=} \left\{\tilde{\mathbf{h}}^{\mathbf{s}}_{[\mu]}\right\}$, and the synthesis $\mathbf{H}_{[\mu]} \stackrel{\text{def}}{=} \left\{\mathbf{h}^{\mathbf{s}}_{[\mu]}\right\}$, $s = 0, ..., S-1$, are p-filter banks with downsampling factor of 2 form PR p-filter banks, which operate in the subspaces $\Pi[N/2^\mu]$ where $\tilde{\mathbf{P}}_{[\mu]}[n]$, $\mu = 0, ...m-1$, and $\mathbf{P}_{[\mu]}[n]$ are their polyphase matrices. Here, $\mathbf{H}_{[\mathbf{0}]} \stackrel{\text{def}}{=} \mathbf{H}$ and $\tilde{\mathbf{H}}_{[0]} \stackrel{\text{def}}{=} \tilde{\mathbf{H}}$ denote the p-filter banks at the initial level, $\tilde{\mathbf{P}}_{[\mathbf{0}]}[n]$ and $\mathbf{P}_{[\mathbf{0}]}[n]$ are their polyphase matrices. The simplest way to define the multilevel polyphase matrices is to define $\tilde{\mathbf{P}}_{[\mu+1]}[n] \stackrel{\text{def}}{=} \tilde{\mathbf{P}}_{[\mu]}[2n]$ and $\mathbf{P}_{[\mu+\mathbf{1}]}[n] \stackrel{\text{def}}{=} \mathbf{P}_{[\mu]}[2n]$, $\mu = 0, ...m-1$.

To increase the redundancy of a signal representation, the frame transform is applied to the low frequency signal $\mathbf{y}^0_{[1]} = \left\{y^0_{[1]}[l]\right\}$, $y^0_{[1]}[l] = \sum_{k=0}^{N-1} \tilde{\psi}^s_{[1]}[k-2l]\, x[k]$ that belongs to $\Pi[N/2]$. Repeating the above reasoning, we get $x^0_{[1]}[k] = \sum_{s=0}^{S-1} \sum_{\lambda=0}^{N/4-1} \left\langle \mathbf{x}, \tilde{\psi}^s_{[2]}[\cdot - 4l]\right\rangle \psi^s_{[2]}[k - 4\lambda]$, where
$\tilde{\psi}^s_{[2]}[\kappa] \stackrel{\text{def}}{=} \sum_{\nu=0}^{N/2-1} \tilde{h}^s_{[1]}[\nu]\, \tilde{\psi}^0_{[1]}[\kappa - 2\nu], \psi^s_{[2]}[k] \stackrel{\text{def}}{=} \sum_{l=0}^{N/2-1} \psi^0_{[1]}[k-2l]\, h^s_{[1]}[l]$, $s = 0, ..., S-1$. The signals $\left\{\tilde{\psi}^s_{[2]}\right\}$ and $\left\{\psi^s_{[2]}\right\}$ are called the analysis and the synthesis discrete time periodic framelets of the second decomposition level, respectively.

The iterated transform with the polyphase matrices $\tilde{\mathbf{P}}_{[\mu]}[n]$ and $\mathbf{P}_{[\mu]}[n]$ leads to the frame expansion of the signal $\mathbf{x} = \mathbf{x}^0_{[m]} + \sum_{\mu=1}^{m} \sum_{s=1}^{S-1} \mathbf{x}^s_{[\mu]}$, where

$$\begin{aligned} x^s_{[m]}[k] &= \textstyle\sum_{l\in\mathbb{Z}} \left\langle \mathbf{x}, \tilde{\psi}^s_{[m]}[\cdot - 2^m l]\right\rangle \psi^s_{[m]}[k - 2^m l],\ s = 0, ..., S-1, \\ x^s_{[\mu]}[k] &= \textstyle\sum_{l=0}^{N/2^\mu-1} \left\langle \mathbf{x}, \tilde{\psi}^s_{[\mu]}[\cdot - 2^\mu l]\right\rangle \psi^s_{[\mu]}[k - 2^\mu l], \quad \mu < m,\ s = 1, ..., S-1. \end{aligned} \tag{4.5}$$

The synthesis and analysis framelets are derived iteratively

$$\psi^s_{[\mu]}[k] \stackrel{\text{def}}{=} \sum_{l=0}^{N/2^{\mu-1}-1} h^s_{[\mu-1]}[l]\, \psi^0_{[\mu-1]}[k - 2^{\mu-1}l], \quad \tilde{\psi}^s_{[\mu]}[k] \stackrel{\text{def}}{=} \sum_{l=0}^{N/2^{\mu-1}-1} \tilde{h}^s_{[\mu-1]}[l]\, \tilde{\psi}^0_{[\mu-1]}[k - 2^{\mu-1}l]. \tag{4.6}$$

5 Design of p-filter banks for frames generation

In this section, we discuss the design of four-channel p-filter banks, which generate the tight and the so-called semi-tight frames in the periodic signals space $\Pi[N]$.

The PR condition for a pair of the analysis $\tilde{\mathbf{H}} = \left\{\tilde{\mathbf{h}}^0, \tilde{\mathbf{h}}^1, \tilde{\mathbf{h}}^2, \tilde{\mathbf{h}}^3\right\}$ and the synthesis $\mathbf{H} = \left\{\mathbf{h^0}, \mathbf{h^1}, \mathbf{h^2}, \mathbf{h^3}\right\}$ p-filter banks is expressed via their polyphase matrices

$$\mathbf{P}[n]\cdot\tilde{\mathbf{P}}[-n]=\begin{pmatrix}\hat{h}_0^0[n]_1 & \hat{h}_0^1[n]_1 & \hat{h}_0^2[n]_1 & \hat{h}_0^3[n]_1\\ \hat{h}_1^0[n]_1 & \hat{h}_1^1[n]_1 & \hat{h}_1^2[n]_1 & \hat{h}_1^3[n]_1\end{pmatrix}\cdot\begin{pmatrix}\hat{\tilde{h}}_0^0[-n]_1 & \hat{\tilde{h}}_1^0[-n]_1\\ \hat{\tilde{h}}_0^1[-n]_1 & \hat{\tilde{h}}_1^1[-n]_1\\ \hat{\tilde{h}}_0^2[-n]_1 & \hat{\tilde{h}}_1^2[-n]_1\\ \hat{\tilde{h}}_0^3[-n]_1 & \hat{\tilde{h}}_1^3[-n]_1\end{pmatrix}=\mathbf{I}_2,\quad n\in\mathbb{Z}. \tag{5.1}$$

The matrix product in Eq. (5.1) can be split into two products. Then,

$$\mathbf{P}[n]\cdot\tilde{\mathbf{P}}[-n]=\mathbf{P}^{01}[n]\cdot\tilde{\mathbf{P}}^{01}[-n]+\mathbf{P}^{23}[n]\cdot\tilde{\mathbf{P}}^{23}[-n]=\begin{pmatrix}1 & 0\\ 0 & 1\end{pmatrix}, \tag{5.2}$$

$$\mathbf{P}^{\mathbf{01}}[n]\stackrel{\text{def}}{=}\begin{pmatrix}\hat{h}_0^0[n]_1 & \hat{h}_0^1[n]_1\\ \hat{h}_1^0[n]_1 & \hat{h}_1^1[n]_1\end{pmatrix},\quad \tilde{\mathbf{P}}^{01}[n]\stackrel{\text{def}}{=}\begin{pmatrix}\hat{\tilde{h}}_0^0[n]_1 & \hat{\tilde{h}}_1^0[n]_1\\ \hat{\tilde{h}}_0^1[n]_1 & \hat{\tilde{h}}_1^1[n]_1\end{pmatrix}$$

$$\mathbf{P}^{23}[n]\stackrel{\text{def}}{=}\begin{pmatrix}\hat{h}_0^2[n]_1 & \hat{h}_0^3[n]_1\\ \hat{h}_1^2[n]_1 & \hat{h}_1^3[n]_1\end{pmatrix}\quad \tilde{\mathbf{P}}^{23}[n]\stackrel{\text{def}}{=}\begin{pmatrix}\hat{\tilde{h}}_0^2[n]_1 & \hat{\tilde{h}}_1^2[n]_1\\ \hat{\tilde{h}}_0^3[n]_1 & \hat{\tilde{h}}_1^3[n]_1\end{pmatrix}.$$

According to Theorem 4.2, a PR pair $\left\{\mathbf{H},\,\tilde{\mathbf{H}}\right\}$ of p-filter banks generate a tight frame if their polyphase matrices are linked as

$$\mathbf{P}[n]=\tilde{\mathbf{P}}[n]^T\Longleftrightarrow\mathbf{P}^{\mathbf{01}}[n]=\tilde{\mathbf{P}}^{\mathbf{01}}[n]^T\quad\text{and}\quad\mathbf{P}^{23}[n]=\tilde{\mathbf{P}}^{23}[n]^T,\quad n\in\mathbb{Z}.$$

Definition 5.1 *Assume that* $\widetilde{\mathbf{P}}[n]$ *and* $\mathbf{P}[n]$ *are the polyphase matrices of the PR pair* $\left\{\tilde{\mathbf{H}},\,\mathbf{H}\right\}$ *of p-filter banks, which generate a bi-frame* $\left\{\tilde{\mathbf{F}},\,\mathbf{F}\right\}$ *in the space* $\Pi[N]$. *If the matrices* $\mathbf{P}^{01}[n]=\tilde{\mathbf{P}}^{01}[n]^T$ and $\mathbf{P}^{23}[n]\neq\tilde{\mathbf{P}}^{23}[n]^T,\quad n\in\mathbb{Z}$, *then the PR frame* $\left\{\tilde{\mathbf{F}},\,\mathbf{F}\right\}$ *is called semi-tight.*

The design of four-channel filter banks begins from a linear phase low-pass filter $\mathbf{h}^0=\tilde{\mathbf{h}}^0$, whose FR $\hat{h}^0[n]=\hat{h}_0^0[n]_1+\omega^{-n}\hat{h}_1^0[n]_1$ is a rational function of $\omega^n=e^{2\pi in/N}$ with real coefficients that has no poles for $n\in\mathbb{Z}$. Assume $\hat{h}^0[n]$ is symmetric about the swap $n\to-n$, which implies that $\hat{h}_0^0[n]_1=\hat{h}_0^0[-n]_1$ and $\omega^{-n}\hat{h}_1^0[n]_1=\omega^n\,\hat{h}_1^0[-n]_1$. The IR $\left\{h^0[k]\right\}$ is symmetric about $k=0$.

In addition, assume that $\mathbf{P}^{01}[n]=\tilde{\mathbf{P}}^{01}[n]^T$ and the product

$$\mathbf{P}^{01}[n]\cdot\mathbf{P}^{01}[-n]=\begin{pmatrix}\alpha[n]_1 & 0\\ 0 & \beta[n]_1\end{pmatrix} \tag{5.3}$$

is a diagonal matrix. The assumption in Eq. (5.3) implies the condition $\hat{h}_0^0[n]_1\hat{h}_1^0[-n]_1+\hat{h}_0^1[n]_1\hat{h}_1^1[-n]_1=0$. The simplest way to satisfy this condition is to define

$$\hat{h}_0^1[n]_1\stackrel{\text{def}}{=}-\hat{h}_1^0[-n]_1,\ \hat{h}_1^1[n]_1\stackrel{\text{def}}{=}h_0^0[-n]_1\Longrightarrow\alpha[n]_1=\beta[n]_1=\left|\hat{h}_0^0[n]_1\right|^2+\left|\hat{h}_1^0[n]_1\right|^2.$$

Due to the symmetry of $\hat{h}^0[n]$, the FR

$$\hat{h}^1[n]=-\hat{h}_1^0[-n]_1+\omega^{-n}\hat{h}_0^0[-n]_1=\omega^{-n}\left(\hat{h}_0^0[n]_1-\omega^{-n}\hat{h}_1^0[n]_1\right)=\omega^{-n}\hat{h}^0[n+N/2]. \tag{5.4}$$

Equation (5.4) implies that the sequence $\omega^n\hat{h}^1[n]$ is symmetric about the swap $n\to-n$ and, consequently, the IR $\left\{h^1[k]\right\}$ is symmetric about $k=1$.

It follows from the assumption in Eq. (5.3) that the product

$$\mathbf{P}^{23}[n]\cdot\tilde{\mathbf{P}}^{23}[-n]=\mathbf{Q}[n]\stackrel{\text{def}}{=}\begin{pmatrix}t[n]_1 & 0\\ 0 & t[n]_1\end{pmatrix},\quad\text{where}\quad t[n]_1\stackrel{\text{def}}{=}1-\left|\hat{h}_0^0[n]_1\right|^2+\left|\hat{h}_1^0[n]_1\right|^2 \tag{5.5}$$

is a diagonal matrix. Thus, the design of the PR p-filter bank is reduced to factorization of the matrix $\mathbf{Q}[n]$.

There are many ways to factorize the matrix $\mathbf{Q}[n]$. One way is to define the matrices $\mathbf{P}^{23}[n]$ and $\tilde{\mathbf{P}}^{23}[n]$ to be diagonal:

$$\mathbf{P}^{23}[n] = \begin{pmatrix} \hat{h}_0^2[n]_1 & 0 \\ 0 & \hat{h}_1^3[n]_1 \end{pmatrix}, \quad \tilde{\mathbf{P}}^{23}[n] \stackrel{\text{def}}{=} \begin{pmatrix} \hat{\tilde{h}}_0^2[n]_1 & 0 \\ 0 & \hat{\tilde{h}}_1^3[n]_1 \end{pmatrix},$$

which means that the odd polyphase components of the p-filters $\tilde{\mathbf{h}}^2$ and $\mathbf{h}^2$ as well as the even polyphase components of the p-filters $\tilde{\mathbf{h}}^3$ and $\mathbf{h}^3$ vanish. Consequently, we have to find four sequences $\hat{h}_0^2[n]_1$, $\hat{\tilde{h}}_0^2[n]_1$, $\hat{h}_1^3[n]_1$ and $\hat{\tilde{h}}_1^3[n]_1$ such that

$$\hat{h}_0^2[n]_1 \, \hat{\tilde{h}}_0^2[n]_1 = \hat{h}_1^3[n]_1 \, \hat{\tilde{h}}_1^3[n]_1 = t[n]_1. \tag{5.6}$$

Tight frame p-filter banks: If the following inequality holds

$$\alpha[n]_1 = \left|h_0^0[n]_1\right|^2 + \left|h_1^0[n]_1\right|^2 \leq 1, \quad n \in \mathbb{Z}, \tag{5.7}$$

then, due to the symmetry of the rational functions $\hat{h}_0^0[n]_1$ and $\hat{h^0}_0[n]_1$, we have
$1 - a[n]_1 = P(\cos 2\pi n/N)/Q(\cos 2\pi n/N)$, where Q is strictly positive and P is non-negative polynomials.

Lemma 5.2 ([23]) *Let* A *be a positive trigonometric polynomial containing only cosines, $A(v) = \sum_{\nu=1}^{M} a_\nu \cos \nu v$, with real coefficients a_ν. Then, there exists a trigonometric polynomial $B(v) = \sum_{\nu=1}^{M} b_\nu \, e^{i\nu v}$ order* M *with real coefficients b_ν such that $|B(v)|^2 = A(v)$.*

Due to Riesz Lemma 5.2, the polynomials can be factorized $P(\cos 2\pi n/N)) = p(\omega^n)\, p(\omega^{-n})$, $Q(\cos 2\pi n/N)) = q(\omega^n)\, q(\omega^{-n})$, where p and q are polynomials with real coefficients and $q(\omega^n)$ does not have roots for $n \in \mathbb{Z}$. Thus, we can define

$$\hat{h}_0^2[n]_1 = \hat{\tilde{h}}_0^2[n]_1 = \hat{h}_1^3[-n]_1 = \hat{\tilde{h}}_1^3[-n]_1 = T[n]_1 \stackrel{\text{def}}{=} \frac{p(\omega^n)}{q(\omega^n)}. \tag{5.8}$$

The PR p-filter bank, whose FR are

$$\begin{array}{ll} \hat{h}^0[n] = \hat{h}_0^0[n]_1 + \omega^{-n}\hat{h}_0^0[n]_1 & \hat{h}^2[n] = T[n]_1, \\ \hat{h}^1[n] = -\hat{h}_1^0[-n]_1 + \omega^{-n}\hat{h}_0^0[-n]_1, & \hat{h}^3[n] = \omega^{-n}T[-n]_1, \end{array}$$

generates a tight wavelet frame in the space $\Pi[N]$. Certainly, the symmetry of the FR $\hat{h}^0[n]$ does not guarantee the symmetry of the FR $\hat{h}^2[n]$ and $\hat{h}^3[n]$.

Semi-tight frame p-filter banks: If the condition Eq. (5.7) is not fulfilled then the sequence $t[n]_1$ can be factorized as $t[n]_1 = T[n]_1 \, \tilde{T}[-n]_1$, where $T[n]_1 \neq \tilde{T}[n]_1$. Thus, we obtain the PR p-filter bank, whose FR are

$$\begin{array}{lll} \hat{h}^0[n] = \hat{h}_0^0[n]_1 + \omega^{-n}\hat{h}_0^0[n]_1 & \hat{h}^2[n] = T^2[n]_1, & \hat{\tilde{h}}^2[n] = \tilde{T}^2[n]_1, \\ \hat{h}^1[n] = -\hat{h}_1^0[-n]_1 + \omega^{-n}\hat{h}_0^0[-n]_1, & \hat{h}^3[n] = \omega^{-n}T^3[n]_1, & \hat{\tilde{h}}^3[n] = \omega^{-n}\tilde{T}^3[n]_1, \end{array} \tag{5.9}$$

where $T^2[n]_1 \, \tilde{T}^2[-n]_1 = T^3[n]_1 \, \tilde{T}^3[-n]_1 = t[n]_1$. The PR p-filter bank defined by Eq. (5.9) genetates a semi-tight in the space $\Pi[N]$.

Remark 5.1 *Since the rational function $t[n]_1$ of ω^n is symmetric about the change $n \to -n$, then it can be factorized into product of two symmetric rational functions $T[n]_1$ and $\tilde{T}[-n]_1$. An additional advantage of the semi-tight design is the option to swap approximation properties between the analysis and the synthesis framelets.*

Interpolating p-filter banks: Assume that the low-pass p-filter $\mathbf{h}^0$ is interpolating and its FR is $\hat{h}^0[n] = (1+\omega^{-n} f[n]_1)/\sqrt{2}$, where the sequence $f[n]_1$ is a rational function of $\omega^n = e^{2\pi i n/N}$ that has no poles as $n \in \mathbb{Z}$ and

$$f[0]_1 = 1, \quad \omega^{-n} f[n]_1 = \omega^n f[-n]_1. \tag{5.10}$$

The sequence $t[n]_1$ to be factorized is

$$t[n]_1 = 1 - \left|\hat{h}_0^0[n]_1\right|^2 + \left|\hat{h}_1^0[n]_1\right|^2 = \frac{W[n]_1}{2}, \quad W[n]_1 \stackrel{\text{def}}{=} 1 - |f[n]_1|^2 = 2\hat{h}^0[n]\,\hat{h}^0[n+N/2]. \tag{5.11}$$

In this case, the polyphase submatrices are

$$\mathbf{P}^{01}[n] = \tilde{\mathbf{P}}^{01}[n]^T = \frac{1}{\sqrt{2}} \begin{pmatrix} 1 & f[n]_1 \\ -f[-n]_1 & 1 \end{pmatrix}, \tag{5.12}$$

$$\mathbf{P}^{\mathbf{23}}[n] = \begin{pmatrix} T^2[n]_1 & 0 \\ 0 & T^3[n]_1 \end{pmatrix} \quad \tilde{\mathbf{P}}^{23}[n] = \begin{pmatrix} \tilde{T}^2[n]_1 & 0 \\ 0 & \tilde{T}^3[n]_1 \end{pmatrix},$$

where $T^2[n]_1\,\tilde{T}^2[-n]_1 = T^3[n]_1\,\tilde{T}^3[-n]_1 = W[n]_1/2$.

6 Restoration of sampled polynomials and discrete vanishing moments

It is apparent that as the FR of a low-pass filter $\mathbf{h}$ at the vicinity of zero becomes flatter, it better restores band-limited signals. To be specific, if $\hat{h}[n] \equiv c$ as $|n| \le n_0$ (up to a period N) and the DFT $\hat{x}[n]$ of a signal $\mathbf{x} \in \Pi[N]$ is zero outside the interval $-n_0 \le n \le n_0$, then application of the p-filter $\mathbf{h}$ restores the signal $\mathbf{x}$ by $\sum_{l=0}^{N-1} h[k-l]\,x[l] = c\,x[k]$.

6.1 Restoration of sampled polynomials

The flatness of the FR of a low-pass filter can be characterized by the difference $\hat{h}[n] - \hat{h}[0]$. Under the assumption that the FR $\hat{h}[n]$ is a rational function of $\omega^n = e^{2\pi i n/N}$, which has no poles while $n \in \mathbb{Z}$, the difference $\hat{h}[n] - \hat{h}[0] = (\omega^n - 1)^m\ \alpha[n]$, where m is a natural number and $\alpha[n]$ is a rational function of ω^n, which has no poles while $n \in \mathbb{Z}$ and $\alpha[0] \neq 0$. As the multiplicity m of the root becomes higher then the FR becomes flatter.

Equation (2.1) implies that the sequence $(\omega^n - 1)^m$ is the DFT of the circular finite difference and $(\omega^n - 1)^m \hat{x}[n] = \hat{\Delta}^m[\mathbf{x}][n]$. The sequence $\{\alpha[n]\}$ can be regarded as the FR of a low-(all-)pass p-filter $\mathbf{a}$. Then, the application of the p-filter $\mathbf{h}$ to a signal $\mathbf{x} \in \Pi[N]$ can be represented as

$$\mathbf{h}\,\mathbf{x} = \hat{h}[0]\,\mathbf{x} + \mathbf{a}\,\Delta^m[\mathbf{x}]. \tag{6.1}$$

Certainly, sampled polynomials do not belong to $\Pi[N]$ and p-filters can not be applied to them. However, the following fact holds, which in a sense is a discrete periodic counterpart of the classical Fix-Strang condition [27].

Proposition 6.1 *Assume that the FR of the low-pass filter* $\mathbf{h}$ *can be represented as* $\hat{h}[n] = \hat{h}[0] + (\omega^n - 1)^m\ \alpha[n]$, *where* m *is some natural number and* $\alpha[n]$ *is a rational function of* ω^n, *which has no poles for* $n \in \mathbb{Z}$ *and* $\alpha[0] \neq 0$. *Assume* $\mathbf{p}$ *is a signal from* $\Pi[N]$, *which coincides with a sampled polynomial* $\mathbf{P}_{m-1}$ *of degree* $m-1$ *at some interval* $p[k] = P_{m-1}[k]$, $k = k_0, ..., k_m$, *where* $m < k_m - k_0 < N$. *Then,* $\sum_{l=0}^{N-1} h[k-l]\,p[l] = \hat{h}[0]\,P_{m-1}[k]$, *as* $k = k_0, ..., k_m - m - 1$.

Proof: Under the conditions of the proposition, the application of the p-filter $\mathbf{h}$ to a signal $\mathbf{x} \in \Pi[N]$ can be represented as in Eq. (6.1). The finite difference of the signal $\mathbf{p}$

$$\Delta^m[\mathbf{p}][k] = \sum_{l=0}^{m} (-1)^l \binom{m}{l} p[k+l] = \Delta^m[\mathbf{P}_{m-1}][k], \text{ as } k = k_0, ..., k_m - m - 1.$$

According to Proposition 2.1, $\Delta^m[\mathbf{P}_{m-1}][k] = 0$. Thus, the statement follows from Eq. (6.1).■

Definition 6.2 *If a low-pass p-filter* $\mathbf{h}$ *satisfies the conditions of Proposition 6.1, then we say that the p-filter* $\mathbf{h}$ *locally restores sampled polynomials of degree* $m-1$.

6.2 Discrete vanishing moments

Proposition 6.3 *Assume that the FR of the high(band)-pass filter* $\mathbf{g}$ *can be represented as* $\hat{g}[n] = (\omega^n - 1)^m \, \alpha[n]$, *where* m *is a natural number and* $\alpha[n]$ *is a rational function of* ω^n, *which has no poles for* $n \in \mathbb{Z}$ *and* $\alpha[0] \neq 0$. *Assume* $\mathbf{p}$ *is a signal from* $\Pi[N]$, *which coincides with a sampled polynomial* $\mathbf{P}_{m-1}$ *of degree* $m-1$ *at some interval* $p[k] = P_{m-1}[k]$, $k = k_0, ..., k_m$, *where* $m < k_m - k_0 < N$. *Then,* $\sum_{l=0}^{N-1} g[k-l]\, p[l] = 0$, $k = k_0, ..., k_m - m - 1$.

Proof: is similar to the proof of Proposition 6.1.

Definition 6.4 *If a high(band)-pass p-filter* $\mathbf{g}$ *satisfies the conditions of Proposition 6.3, we say that the p-filter* $\mathbf{g}$ *locally eliminates sampled polynomials of degree* $m-1$. *If a framelet* $\psi_{[1]}[k] \stackrel{\text{def}}{=} g[k]$, $k \in \mathbb{Z}$, *we say that the framelet* $\psi_{[1]}$ *has* m *local discrete vanishing moments (LDVM).*

Remark 6.1 *The statements of Propositions 6.1 and 6.3 concerning the low-pass* $\mathbf{h}$ *and high-pass* $\mathbf{g}$ *filters, respectively, remain true if the frequency responses are represented as*

$$\hat{h}[n] = \hat{h}[0] + \sin^m \frac{\pi n}{N} \, \bar{\alpha}[n], \quad \hat{g}[n] = \sin^m \frac{\pi n}{N} \, \bar{\alpha}[n],$$

where m *is a natural number and* $\bar{\alpha}[n]$ *is a rational function of* ω^n, *which has no poles for* $n \in \mathbb{Z}$ *and* $\bar{\alpha}[0] \neq 0$.

Restoration of polynomials by low-pass filters coupled with their elimination by respective high- and band-pass filters constituting the p-filter banks provide a sparse representation of signals/images, which is important, for example, for data compression and signals/images restoration.

7 Spline based low- and high-pass p-filters

Assume that the FR of a low-pass interpolating p-filter $\mathbf{h}^0$ operating in $\Pi[N]$ is presented by $\tilde{h}^0[n] = (1 + \omega^{-n} f[n]_1)/\sqrt{2}$. The FR of the corresponding high-pass p-filter $\mathbf{h}^1$ is $\tilde{h}^1[n] = \omega^{-n}(1 - \omega^{-n} f[n]_1)/\sqrt{2}$. Then, the DFT of the signal $\mathbf{y} = \mathbf{h}^1 \mathbf{x}$, where $\mathbf{x} \in \Pi[N]$, is

$$\hat{y}[n] = \frac{1}{\sqrt{2}} \left(-f[-n]_1 \, \hat{x}_0[n]_1 + \omega^{-2n} \hat{x}_1[n]_1 \right) + \frac{\omega^{-n}}{\sqrt{2}} \left(\hat{x}_0[n]_1 - \hat{f}[-n]_1 \, \hat{x}_1[n]_1 \right).$$

Denote by $\mathbf{f}$ the p-filter in $\Pi[N/2]$ whose FR is $f[-n]_1$ and by $\bar{\mathbf{x}}_1 \stackrel{\text{def}}{=} \{x[2k-1]\}$ the shifted odd polyphase component, while $\mathbf{x}_1 \stackrel{\text{def}}{=} \{x[2k+1]\}$. Then, the polyphase components of $\mathbf{y}$ are $\mathbf{y}_0 = (\bar{\mathbf{x}}_1 - \mathbf{f}\,\mathbf{x}_0)/\sqrt{2}$, $\mathbf{y}_1 = (\mathbf{x}_0 - \mathbf{f}\,\mathbf{x}_1)/\sqrt{2}$.

In order for the high-pass filter to eliminate smooth signals (for example, fragments of polynomials), the p-filter $\mathbf{f}$ should be "predictive" in a sense that its application to the even polyphase component of the signal should "predict" the odd polyphase component and vice versa.

Polynomial splines are natural sources to derive prediction p-filters from. The idea is to construct the spline (quasi-)interpolating the even samples of a signal and to predict the odd samples of the spline's values in the midpoints between the interpolation points. Such an approach was explored for the design of the biorthogonal wavelet transforms in [2, 5, 4]. The prediction filters derived from the discrete splines were used for the design of non-periodic interpolating wavelet frames [6, 7] with three-channel filter banks.

7.1 Prediction p-filters derived from splines

A spline of order p on the grid $\{t_k\}$ is a function that has $p-2$ continuous derivatives. At the intervals (t_k, t_{k+1}) between the grid points, the spline of order p coincides with polynomials $\mathbf{P}_k^{p-1}$ of degree $p-1$.

7.1.1 Periodic interpolating splines

Denote by $\mathbf{S}_K^p$ the space of splines of order $p \in \mathbb{N}$ defined on the uniform grid $\{k\}$, which are periodic with the period $K = N/2 = 2^{j-1}$. A basis in this space is constituted by shifts of the so-called B-splines. The K-periodic B-spline $B^1(t)$ of first order is the periodization of the compactly supported function $\beta^1(t)$

$$\beta^1(t) \stackrel{\text{def}}{=} \begin{cases} 1, & \text{if } t \in (-1/2, 1/2) \\ 0, & \text{otherwise,} \end{cases} \qquad B^1(t) \stackrel{\text{def}}{=} \sum_{l \in \mathbb{Z}} \beta^1(t + Kl) = \frac{1}{K} \sum_{n \in \mathbb{Z}} e^{2\pi i n t/K} \, \frac{\sin \pi n/K}{\pi n/K}.$$

The B-splines of higher order are defined iteratively via the circular convolution $B^p(t) \stackrel{\text{def}}{=} B^1 \circledast B^{p-1}(t)$. The B-spline $B^p(t)$ is supported on the interval $-p/2, p/2$ (up to periodization), is strictly positive inside this interval and is symmetric about zero, where it has its single maximum.

Any spline $S^p(t)$ from $\mathbf{S}_K^p$ is represented as

$$S^p(t) = \sum_{k=0}^{K-1} q[k] \, B^p(t-k). \tag{7.1}$$

If the spline $S^p(t)$ interpolates the even polyphase component $\mathbf{x}_0 = \{x[2l]\}$ of a signal $\mathbf{x} \in \Pi[N]$ then its coefficients $q[k]$ can be explicitly calculated via the DFT

$$\begin{gathered} S^p(l) = \textstyle\sum_{k=0}^{K-1} q[k] \, B^p(l-k) = x_0[l] \Longleftrightarrow \hat{q}[n]_1 u^p[n]_1 = \hat{x}_0[n]_1, \\ u^p[n]_1 \stackrel{\text{def}}{=} \textstyle\sum_{k=0}^{K-1} \omega^{2nk} \, B^p(k) > 0 \Longrightarrow \hat{q}[n]_1 = \hat{x}_0[n]_1 / u^p[n]_1. \end{gathered} \tag{7.2}$$

The $K = N/2$-periodic sequence $u^p[n]_1$, which is the DFT of the sampled B-spline $\{B^p(k)\}$, is strictly positive. Due to symmetry and positiveness of the B-spline, $u^p[n]_1 = u^p[-n]_1$, thus it is a cosine polynomial with positive coefficients. It is symmetric about $K/2$, where it has its single minimum. The maximal value of $u^p[n]_1$ is 1 being reached when $n = 0$.

Approximation properties of interpolating splines are well investigated. In particular, the non-periodic interpolating spline of order p, which consists of piece-wise polynomials of degree $p-1$, restores these polynomials. It means that splines of order p, which interpolate a polynomial of degree $p-1$, coincides with this polynomial. For periodic splines, this property holds locally. This observation justifies the choice of interpolating splines as a source for the design of prediction filters.

To be specific, if the spline $S^p(t) \in \mathbf{S}_K^p$, given in Eq. (7.1), interpolates the even polyphase component $\mathbf{x}_0 = \{x[2l]\}$ of a signal $\mathbf{x} \in \Pi[N]$, then the odd polyphase component $\mathbf{x}_1 = \{x[2l+1]\}$ is predicted as the midpoint values of the spline $\sigma[l] \stackrel{\text{def}}{=} S^p(l+1/2) = \sum_{k=0}^{K-1} q[k] \, B^p(l+1/2-k)$, whose DFT is $\hat{\sigma}[n]_1 = \hat{q}[n]_1 \, v^p[n]_1 = \frac{v^p[n]_1}{u^p[n]_1} \, \hat{x}_0[n]_1$, where $v^p[n]_1 \stackrel{\text{def}}{=} \sum_{k=0}^{K-1} \omega^{2nk} \, B^p(l+1/2)$ is the DFT of the B-spline $\{B^p(k+1/2)\}$ sampled at midpoints between grid points.

The continuous counterparts of the sequences $u^p[n]_1$ and $v^p[n]_1$, which are the discrete-time Fourier transforms of the non-periodic B-splines, were introduced and studied in [25]. Some additional properties of

the sequences $u^p[n]_1$ and $v^p[n]_1$ are established in [30, 2]. Denote

$$f_c^p[n]_1 \stackrel{\text{def}}{=} \frac{v^p[n]_1}{u^p[n]_1}. \tag{7.3}$$

Obviously, the sequence $f_c^p[n]_1$ satisfies the conditions in Eq. (5.10).

Proposition 7.1 ([2]) *If the spline order is $p = 2r$ or $p = 2r - 1$ then*

$$\hat{h}^0[n] \stackrel{\text{def}}{=} \frac{1}{\sqrt{2}}\left(1 + \omega^{-n} f_c^p[n]_1\right) = \hat{h}[0] + \sin^{2r}\frac{\pi n}{N}\,\chi^p[n] \tag{7.4}$$

$$\hat{h}^1 \stackrel{\text{def}}{=} \frac{\omega^{-n}}{\sqrt{2}}\left(1 - \omega^{-n} f_c^p[-n]_1\right) = \sin^{2r}\frac{\pi n}{N}\,\gamma^p[n], \tag{7.5}$$

where r is a natural number and $\chi^p[n]$ and $\gamma^p[n]$ are rational functions of ω^n, which have no poles for $n \in \mathbb{Z}$ and no root at $n = 0$.

This proposition coupled with Propositions 6.1 and 6.3 and Remark 6.1 imply the following Corollary.

Corollary 7.2 *The low-pass $\mathbf{h}^0$ and the high-pass $\mathbf{h}^1$ p-filters, whose FR are given in Eqs. (7.4) and (7.5), respectively, locally restore and eliminate sampled polynomials of degree $2r - 1$, respectively.*

Therefore, the p-filter $\mathbf{f}_c^p$, whose FR $f_c^p[n]_1$ is defined by Eq. (7.3), is a proper candidate to be utilized as a prediction p-filter.

Remark 7.1 *It is emphasized that the p-filters derived from the odd order $2r - 1$ splines restore (eliminate) sampled polynomials of the same $2r - 1$ degree as the the p-filters derived from the even order $2r$ splines. This is a consequence of the so-called super-convergence property of the odd order interpolating splines [30], which claims that the approximation order of such splines at the midpoints between the interpolation points is higher than those at the remaining points of the intervals between the interpolation points.*

7.1.2 Examples of spline based p-filters

The sequences $\{v^p[n]_1\}$ and $\{u^p[n]_1\}$, whose ratio constitute the FR $f_c^p[n]_1$ of a prediction p-filter $\mathbf{f}_c^p$, are calculated explicitly via the DFT of the B-splines sampled at the points $\{k + 1/2\}$ and $\{k\}$, respectively. Table 1 presents the sequences $\{B^p(k)\}$ and $\{B^p(k + 1/2)\}$ for different p values.

k	-4	-3	-2	-1	0	1	2	3
$B^2(k)$	0	0	0	0	1	0	0	0
$B^3(k) \times 8$	0	0	0	1	6	1	0	0
$B^4(k) \times 6$	0	0	0	1	4	1	0	0
$B^5(k) \times 384$	0	0	1	76	230	76	1	0
$B^6(k) \times 120$	0	0	1	26	66	26	1	0
$B^7(k) \times 46080$	0	1	722	10543	23548	10543	722	1
$B^2(k + 1/2) \times 2$	0	0	0	1	1	0	0	0
$B^3(k + 1/2) \times 2$	0	0	0	1	1	0	0	0
$B^4(k + 1/2) \times 48$	0	0	1	23	23	1	0	0
$B^5(k + 1/2) \times 24$	0	0	1	11	11	1	0	0
$B^6(k + 1/2) \times 3840$	0	1	237	1682	1682	237	1	0
$B^7(k + 1/2) \times 720$	0	1	57	302	302	57	1	0

Table 1: Sampled B-splines $\{B^p(k)\}$ and $\{B^p(k + 1/2)\}$.

Linear spline $p = 2$**:** $u^2[n]_1 = 1, \quad v^2[n]_1 = (1+\omega^{2n})/2, \quad f_c^2[n]_1 = (1+\omega^{2n})/2,$

$$\hat{h}^0[n] \stackrel{\text{def}}{=} \frac{1}{\sqrt{2}}\left(1+\omega^{-n} f_c^2[n]_1\right) = \sqrt{2}\,\cos^2\frac{\pi n}{N}, \quad \hat{h}^1[n] = \omega^{-n}\sqrt{2}\,\sin^2\frac{\pi n}{N}. \tag{7.6}$$

Quadratic interpolating spline $p = 3$**:**

$$\begin{aligned} u^3[n]_1 &= \frac{\omega^{2n}+6+\omega^{-2n}}{8} = 1-\frac{1}{2}\sin^2\frac{2\pi n}{N} = \cos^4\frac{\pi n}{N}+\sin^4\frac{\pi n}{N}, \quad v^3[n]_1 = \frac{1+\omega^{2n}}{2}, \\ f_c^3[n]_1 &= 4\frac{1+\omega^{2n}}{\omega^{2n}+6+\omega^{-2n}} = \omega^n\,\frac{\cos^4\pi n/N-\sin^4\pi n/N}{\cos^4\pi n/N+\sin^4\pi n/N}, \\ \hat{h}^0[n] &= \sqrt{2}\,\frac{\cos^4\pi n/N}{\cos^4\pi n/N+\sin^4\pi n/N}, \quad \hat{h}^1[n] = \omega^{-n}\sqrt{2}\,\frac{\sin^4\pi n/N}{\cos^4\pi n/N+\sin^4\pi n/N}. \end{aligned} \tag{7.7}$$

Cubic interpolating spline $p = 4$**:**

$$\begin{aligned} f_c^4[n]_1 &= \frac{\omega^{4n}+23\omega^{2n}+23+\omega^{-2n}}{8(\omega^{2n}+4+\omega^{-2n})}, \\ \hat{h}^0[n] &= \sqrt{2}\,\frac{\cos^4\pi n/N\,(2+\cos 2\pi n/N)}{2+\cos 4\pi n/N}, \quad \hat{h}^1[n] = \omega^{-n}\sqrt{2}\,\frac{\sin^4\pi n/N\,(2+\cos 2\pi n/N)}{2+\cos 4\pi n/N}. \end{aligned} \tag{7.8}$$

Comment We observe that the high-pass p-filters $\mathbf{h}^1$ derived either from the quadratic or from the cubic splines locally eliminate sampled cubic polynomials. However, the structure of the quadratic FR is much simpler than the cubic FR. Therefore, in many applications the p-filters derived from quadratic spline are advantageous over the cubic spline p-filters.

Interpolating spline of fourth degree $p = 5$**:**

$$f_c^5[n]_1 = 16\,\frac{\omega^{4n}+11\omega^{2n}+11+\omega^{-2n}}{\omega^{4n}+76\omega^{2n}+230+76\omega^{-2n}+\omega^{-4n}}. \tag{7.9}$$

It is readily verified that the low- and high-pass p-filters locally restore and eliminate sampled polynomials of fifth degree, respectively.

The p-filters, originated from higher order splines, are designed by the application of the DFT to the sampled B-splines.

7.2 Examples of p-FIR p-filters

The IR of all the p-filters introduced in Section 7.1, except for the linear spline p-filters, are infinite, that is they occupy the whole $\mathbb{Z}$. In this section, we introduce a few p-filters, whose IR are finite up to periodization (p-FIR p-filters). One such p-filters is originated from the linear interpolating spline. Another way to design the p-FIR p-filters is to use the splines, which quasi-interpolate rather that interpolate the even polyphase component of a signal $\mathbf{x}$ and to predict the odd polyphase component by the spline's values at the midpoints between the grid nodes. The quasi-interpolating splines are studied in [29, 3]. We describe design of the p-FIR p-filters originating from the quadratic splines. Design of p-filters using quasi-interpolating splines of higher order is similar.

7.2.1 Quadratic quasi-interpolating spline

The quadratic spline, which interpolates the even polyphase component $\mathbf{x}_0$ of a signal $\mathbf{x}_0$, is represented as $S^3(t) = \sum_{k=0}^{N/2-1} q[k]\, B^3(t-k)$, where, due to Eqs. (7.2) and (7.7), the DFT of the coefficients is

$$\hat{q}[n]_1 = \frac{\hat{x}_0[n]_1}{u^3[n]_1} = \frac{\hat{x}_0[n]_1}{1 - \frac{1}{2}\,\sin^2 2\pi n/N} = \hat{x}_0[n]_1 \sum_{l=0}^{\infty} \frac{1}{2^l}\,\sin^{2k}\frac{2\pi n}{N}. \tag{7.10}$$

Two initial terms in the series in Eq. (7.10) are taken and denoted as

$$U^3[n]_1 \stackrel{\text{def}}{=} 1 + \frac{1}{2}\,\sin^2\frac{2\pi n}{N} = \frac{-\omega^{2n} + 10 - \omega^{-2n}}{8}. \tag{7.11}$$

The spline $S^3(t) = \sum_{k=0}^{N/2-1} q[k]\, B^3(t-k)$, where the DFT of the coefficients $\hat{q}[n]_1 = \hat{x}_0[n]_1 U^3[n]_1$, is called the quadratic spline quasi-interpolating the signal $\mathbf{x}_0 \in \Pi[N/2]$. Denote the values of the spline $s_0[k] \stackrel{\text{def}}{=} S^3(k)$ and $s_1[k] \stackrel{\text{def}}{=} S^3(k+1/2), \kappa \in \mathbb{Z}$. Then, the DFT $\hat{s}_0[n]_1 = g_q^3[n]_1\, \hat{x}_0[n]_1$ and $\hat{s}_1[n]_1 = f_q^3[n]_1\, \hat{x}_0[n]_1$, where

$$\begin{gathered} g_q^3[n]_1 = u^3[n]_1\, U^3[n]_1 = \left(-\omega^{-4n} + 4\omega^{-2n} + 58 + 4\omega^{2n} - \omega^{4n}\right)/64, \\ f_q^3[n]_1 = v^3[n]_1\, U^3[n]_1 = \left(-\omega^{-2n} + 9 + 9\omega^{2n} - \omega^{4n}\right)/16. \end{gathered} \tag{7.12}$$

We define two types of low- and high-pass p-filters.

Non-interpolating low-pass p-filter Define the p-filters by their FR:

$$\begin{aligned} &\hat{h}^0[n] \stackrel{\text{def}}{=} \frac{1}{\sqrt{2}}\,\left(g_q^3[n]_1 + \omega^{-n} f_q^3[n]_1\right) = \frac{1}{\sqrt{2}}\,\cos^4\frac{\pi n}{N}\left(3 - \cos\frac{2\pi n}{N}\right) \\ &= \hat{h}^0[0] - \sqrt{2}\,\sin^4\frac{\pi n}{N}\left(5 + 4\cos\frac{2\pi n}{N} + \cos^2\frac{2\pi n}{N}\right), \\ &\hat{h}^1[n] = \omega^{-n}\hat{h}^0[n+N/2] = \frac{\omega^{-n}}{\sqrt{2}}\,\sin^4\frac{\pi n}{N}\left(3 + \cos\frac{2\pi n}{N}\right). \end{aligned} \tag{7.13}$$

The IR of the p-filters $\mathbf{h}^0$ and $\mathbf{h}^1$ comprise nine terms (up to periodization). The low-pass $\mathbf{h}^0$ and the high-pass $\mathbf{h}^1$ p-filters locally restore and eliminate sampled cubic polynomials, respectively.

Intrepolating low-pass p-filter: The same approximation order can be achieved by p-filters, which have shorter IR. For this, the low-pass p-filter $\mathbf{h}^0$ is defined to be interpolating:

$$\begin{aligned} &\hat{h}^0[n] \stackrel{\text{def}}{=} \frac{1}{\sqrt{2}}\,\left(1 + \omega^{-n} f_q^3[n]_1\right) = \sqrt{2}\,\cos^4\frac{\pi n}{N}\left(1 + 2\sin^2\frac{\pi n}{N}\right) = \hat{h}^0[0] - \sqrt{2}\,\sin^4\frac{\pi n}{N}\left(2 + \cos^2\frac{\pi n}{N}\right), \\ &\hat{h}^1[n] = \omega^{-n}\hat{h}^0[n+N/2] = \omega^{-n}\sqrt{2}\,\sin^4\frac{\pi n}{N}\left(1 + 2\cos^2\frac{\pi n}{N}\right). \end{aligned} \tag{7.14}$$

The IR of the p-filters $\mathbf{h}^0$ and $\mathbf{h}^1$ comprise five terms (up to periodization). The low-pass $\mathbf{h}^0$ and the high-pass $\mathbf{h}^1$ p-filters locally restore and eliminate sampled cubic polynomials, respectively.

Like the interpolating spline, the quadratic quasi-interpolating spline possesses the super-convergence property at midpoints between grid nodes. This is the reason why the p-filters and $\mathbf{h}^0$ and $\mathbf{h}^1$ locally restore and eliminate sampled cubic polynomials, respectively.

7.2.2 Pseudo-spline p-filters

A family of linear phase FIR low-pass filters is introduced in [9] for non-periodic setting. In the periodic case, the design starts from the obvious identity

$$1 = \left(\cos^2 \frac{\pi n}{N} + \sin^2 \frac{\pi n}{N}\right)^{m+l}, \quad m, l \in \mathbb{N}. \tag{7.15}$$

The FR of the low-pass p-filter $\mathbf{h}^0$ is derived by summation of the first $l+1$ terms of the binomial expansion in Eq. (7.15):

$$\hat{h}^0[n] = \sqrt{2} \cos^{2m} \frac{\pi n}{N} \sum_{j=0}^{l} \binom{m+l}{j} \sin^{2j} \frac{\pi n}{N} \cos^{2(l-j)} \frac{\pi n}{N}. \tag{7.16}$$

Example: $m = 2,\ l = 1$

$$\hat{h}^0[n] = \sqrt{2} \cos^4 \frac{\pi n}{N} \left(\cos^2 \frac{\pi n}{N} + 3 \sin^2 \frac{\pi n}{N}\right). \tag{7.17}$$

We observe that the filter $\mathbf{h}^0$ defined by Eq. (7.17) is the same as the interpolating p-filter derived from the quadratic quasi-interpolating spline, whose FR is given by Eq. (7.14).

Example from [9]: $m = 3,\ l = 1$

$$\hat{h}^0[n] = \sqrt{2} \cos^6 \frac{\pi n}{N} \left(1 + 3 \sin^2 \frac{\pi n}{N}\right), \quad \hat{h}^1[n] = \omega^{-n} \sqrt{2} \sin^6 \frac{\pi n}{N} \left(1 + 3 \cos^2 \frac{\pi n}{N}\right). \tag{7.18}$$

$$\hat{h}^0[n] - \hat{h}^0[0] = \sqrt{2} \sin^2 \frac{\pi n}{N} \left(3 \cos^6 \frac{\pi n}{N} + \cos^4 \frac{\pi n}{N} + \cos^2 \frac{\pi n}{N} + 1\right).$$

Proposition 6.1 implies that the low-pass p-filter $\mathbf{h}^0$ locally restores only first degree sampled polynomials. However, the high-pass p-filter $\mathbf{h}^1$ locally eliminates fifth degree sampled polynomials. Unlike all the previous examples, the p-filter $\mathbf{h}^0$ is not interpolating. The IR of the filters $\mathbf{h}^0$ and $\mathbf{h}^1$ comprises nine terms (up to periodization).

8 Four-channel p-filter banks using spline filters

In this section, we present a few examples of PR four-channel p-filter banks, which generate tight and semi-tight frames in the space $\Pi[N]$ of N-periodic discrete-time signals. In almost all the forthcoming examples, the low-pass p-filters are interpolating. The design scheme was described in Section 5.

If the low-pass p-filter is interpolating then the polyphase submatrices of the four-channel PR p-filter bank are presented in Eq. (5.12). In this case, once the prediction p-filter $\mathbf{f}$ is available, the design of the p-filter bank is reduced to sequence factorization $W[n]_1 \stackrel{\text{def}}{=} 1 - |f[n]_1|^2 = A[n]_1 \tilde{A}[-n]_1$. Once the factorization is accomplished, the FR of the band-pass p-filters $\widetilde{\mathbf{h}^s}$ and $\mathbf{h}^s,\ s = 2, 3$, are

$$\hat{h}^2[n] = \frac{A[n]_1}{\sqrt{2}}, \quad \hat{h}^3[n] = -\omega^{-n} \frac{\tilde{A}[-n]_1}{\sqrt{2}}, \quad \hat{\tilde{h}}^2[n] = \frac{\tilde{A}[n]_1}{\sqrt{2}}, \quad \hat{\tilde{h}}^3[n] = -\omega^{-n} \frac{A[-n]_1}{\sqrt{2}}. \tag{8.1}$$

The PR pair $\left\{\tilde{\mathbf{H}}, \mathbf{H}\right\}$ of the p-filter banks, where $\tilde{\mathbf{H}} = \left\{\mathbf{h}^0, \mathbf{h}^1, \tilde{\mathbf{h}}^2, \tilde{\mathbf{h}}^3\right\}$ and $\tilde{\mathbf{H}} = \left\{\mathbf{h}^0, \mathbf{h}^1, \mathbf{h}^2, \mathbf{h}^3\right\}$ generates a semi-tight frame in $\Pi[N]$. When $A[n]_1 = \tilde{A}[-n]_1$, the p-filter bank $\mathbf{H}$ generates a tight frame.

The impulse and magnitude responses of PR p-filter banks $\mathbf{H} = \{\mathbf{h}^s\},\ s = 0, 1, 2, 3$, which generate tight frames, are displayed in Fig. 8.7.

The impulse and magnitude responses of p-filters $\tilde{\mathbf{h}}^s$ and $\mathbf{h}^s,\ s = 2, 3$, which, together with the p-filters $\mathbf{h}^s,\ s = 0, 1$, generate semi-tight frames, are displayed in Figs. 8.1–8.6. All the Figs. 8.1–8.6, except for Fig. 8.4, are structured identically. Left pictures display the IR of the p-filters in the following order: Left

to right $\mathbf{h}^2 \longrightarrow \tilde{\mathbf{h}}^2 \longrightarrow \mathbf{h}^3 \longrightarrow \tilde{\mathbf{h}}^3$. Right pictures display the MR of $\mathbf{h}^2$ and $\tilde{\mathbf{h}}^3$ (which coincide with each other) (dashed lines), and the MR of $\tilde{\mathbf{h}}^2$ and $\mathbf{h}^3$ (which coincide with each other) (solid line). Top pair of pictures illustrates the p-filters arising from the symmetric factorization, while the bottom pair does the same when the anti symmetric factorization is the the case. Figure 8.4 comprises only one pair of pictures, which correspond to the symmetric factorization.

Recall that the IR of the p-filters $\tilde{\mathbf{h}}^s$ and $\mathbf{h}^s$, $s = 0, 1, 2, 3$, are the framelets $\tilde{\psi}^s_{[1]}$ and $\psi^s_{[1]}$ of the first level, respectively.

8.1 Four-channel p-filter banks with p-FIR p-filters

A few examples of p-filter banks are given in this section,.

Linear spline: The prediction p-filter is $f^2_c[n]_1 = (1 + \omega^{2n})/2$. Thus,

$$W[n]_1 = \frac{-\omega^{2n} + 2 - \omega^{-2n}}{4} = |A[n]_1|^2, \quad A[n]_1 = \frac{1 - \omega^{2n}}{2}. \tag{8.2}$$

The p-filters $\mathbf{h}^2$ and $\mathbf{h}^3$, whose FR are defined in Eq. (8.1) with $\tilde{A}[n]_1 = A[n]_1$, together with the p-filters $\mathbf{h}^0$ and $\mathbf{h}^1$ defined in Eq. (7.6), constitute a p-filter bank that generates a tight frame. The p-filter $\mathbf{h}^0$ locally restores the sampled polynomials of the first degree while the p-filter $\mathbf{h}^1$ locally eliminates them. The p-filters $\mathbf{h}^3$ and $\mathbf{h}^2$ eliminate only constants. The framelet $\psi^1_{[1]}$, which is the IR of the p-filter $\mathbf{h}^1$, respectively, has two LDVM. Either of the framelets $\psi^3_{[1]}$ and $\psi^2_{[1]}$ has one LDVM. They are antisymmetric.

The IR of the p-filters $\mathbf{h}^s$, $s = 0, 1, 2, 3$, and their magnitude responses are displayed in Fig. 8.7 (top line).

Quadratic quasi-interpolating spline (interpolating low-pass p-filter): The FR of the prediction p-filter $\mathbf{f}$ of low- and high-pass p-filters $\mathbf{h}^0$ and $\mathbf{h}^1$ are given in Eqs. (7.12) and (7.14), respectively. Then the sequence $W[n]_1$ to be factorized is

$$W[n]_1 = \left(\frac{\omega^{2n} - 2 + \omega^{-2n}}{16}\right)^2 \Gamma^4_c[n]_1, \quad \Gamma^4_c[n]_1 \stackrel{\text{def}}{=} -\omega^{2n} + 14 - \omega^{-2n}. \tag{8.3}$$

The following factorization modes $W[n]_1 = A[n]_1\, \tilde{A}[-n]_1$ are possible:

1. Non-symmetric factorization $W[n]_1 = A[n]_1\, A[-n]_1$, , where

$$A[n]_1 = \frac{(\omega^{-2n} - 2 + \omega^{2n})\,(1 - q\,\omega^{2n})}{16\sqrt{q}}, \quad q = 7 - 4\sqrt{3}. \tag{8.4}$$

   The FR of the p-filters $\mathbf{h}^2$ and $\mathbf{h}^3$ are defined in Eq. (8.1) with $\tilde{A}[n]_1 = A[n]_1$.

   The p-filter bank $\mathbf{H} = \{\mathbf{h}^s\}$, $s = 0, 1, 2, 3$, generates a tight frame. The framelet $\psi^1_{[1]}$ has four LDVM, while $\psi^2_{[1]}$ and $\psi^3_{[1]}$ have two. The IR of the p-filters $\mathbf{h}^s$, $s = 0, 1, 2, 3$, and their MR are displayed in Fig. 8.7 (second from top). The IR of the p-filters $\mathbf{h}^2$ and $\mathbf{h}^3$ are nonsymmetric. Their magnitude responses are equal to each other but their phase responses are different.

2. Symmetric factorization of $W[n]_1 = A[n]_1\, \tilde{A}[-n]_1$, which provides equal number (two) of LDVM to the analysis and to the synthesis framelets:

$$\tilde{A}[n]_1 = \frac{\left(\omega^{-2n} - 2 + \omega^{2n}\right)}{4}, \quad A[n]_1 = \frac{\left(\omega^{-2n} - 2 + \omega^{2n}\right)\, \Gamma^4_c[n]_1}{64}. \tag{8.5}$$

   The FR of the p-filters $\tilde{\mathbf{h}}^s$ and $\mathbf{h}^s$, $s = 2, 3$, are defined in Eq. (8.1).

3. Antisymmetric factorization of $W[n]_1 = A[n]_1\,\tilde{A}[-n]_1$, which assigns three LDVM to the analysis framelet $\widetilde{\psi^2_{[1]}}$ leaving only one LDVM to the synthesis framelet $\psi^2_{[1]}$ and vice versa for the framelets $\tilde{\psi}^3_{[1]}$ and $\psi^3_{[1]}$:

$$\tilde{A}[n]_1 = \frac{\omega^{4n} - 3\omega^{2n} + 3 - \omega^{-2n}}{8}, \quad A[n]_1 = \frac{\left(1 - \omega^{2n}\right)\,\Gamma^4_c[n]_1}{32}. \tag{8.6}$$

The FR of the p-filters $\tilde{\mathbf{h}}^s$ and $\mathbf{h}^s$, $s = 2, 3$, are defined in Eq. (8.1). Figure 8.1 displays the IR of the p-filters $\tilde{\mathbf{h}}^s$ and $\mathbf{h}^s$, $s = 2, 3$, which are the discrete time framelets of the first level and their MR.

Figure 8.1: Impulse (left) and magnitude responses (right) of the p-filters $\tilde{\mathbf{h}}^s$ and $\mathbf{h}^s$, $s = 2, 3$, derived from quadratic quasi-interpolating splines (interpolating low-pass p-filter)

Quadratic quasi-interpolating spline (non-interpolating low-pass p-filter): The p-filters $\mathbf{h}^0$ and $\mathbf{h}^1$ are defined in Eq. (7.13). We have

$$t[n]_1 \stackrel{\text{def}}{=} 1 - |h^0_0[n]_1|^2 - |h^0_1[n]_1|^2 = \frac{2(\omega^{2n} - 2 + \omega^{-2n})^2\,T[n]_1}{128^2},$$
$$T[n]_1 \stackrel{\text{def}}{=} -\omega^{4n} - 12\omega^{2n} + 346 - 12\omega^{-2n} - \omega^{-4n}.$$

1. Non-symmetric factorization $t[n]_1 = A[n]_1\,A[-n]_1$:

$$A[n]_1 = \frac{\sqrt{2}\,(\omega - 2 + \omega^{-1})(1 - \alpha_1\omega^{2n})(1 + \alpha_2\omega^{2n})}{128\sqrt{\alpha_1\,\alpha_2}}, \tag{8.7}$$
$$\alpha_1 = 0.07395375302024236412202494176 4069, \quad \alpha_2 = 0.03912854562754878052646969481 2049.$$

The FR of the p-filters $\mathbf{h}^2$ and $\mathbf{h}^3$ are defined in Eq. (8.1) with $\tilde{A}[n]_1 = A[n]_1$. The p-filter bank $\mathbf{H} = \{\mathbf{h}^s\}$, $s = 0, 1, 2, 3$, generates a tight frame. The framelet $\psi^1_{[1]}$ has four LDVM, while $\psi^2_{[1]}$ and $\psi^3_{[1]}$ have two. The IR of the p-filters $\mathbf{h}^s$, $s = 0, 1, 2, 3$, and their MR are displayed in Fig. 8.7 (third from top).

2. Symmetric factorization $t[n]_1 = A[n]_1\,\tilde{A}[-n]_1$:

$$A[n]_1 = \frac{\sqrt{2}(-\omega^{2n} + 2 - \omega^{-2n})\,T[n]_1}{2048}, \quad \tilde{A}[n]_1 = \frac{\sqrt{2}(-\omega^{2n} + 2 - \omega^{-2n})}{4}. \tag{8.8}$$

3. Antisymmetric factorization of $t[n]_1 = A[n]_1\,\tilde{A}[-n]_1$, which assigns three LDVM to the analysis framelet $\tilde{\psi}^2_{[1]}$ leaving only one LDVM to the synthesis framelet $\psi^2_{[1]}$ and vice versa for the framelets $\tilde{\psi}^3_{[1]}$ and $\psi^3_{[1]}$:

$$\tilde{A}[n]_1 = \sqrt{2}\,\frac{\omega^{4n} - 3\omega^{2n} + 3 - \omega^{-2n}}{8}, \quad A[n]_1 = \sqrt{2}\,\frac{\left(1 - \omega^{2n}\right)\,T[n]_1}{1024}. \tag{8.9}$$

The FR of the p-filters $\tilde{\mathbf{h}}^s$ and $\mathbf{h}^s$, $s = 2, 3$, are defined in Eq. (8.1). Figure 8.2 displays the IR of the p-filters $\tilde{\mathbf{h}}^s$ and $\mathbf{h}^s$, $s = 2, 3$, which are the discrete time framelets of the first level, and their MR.

Figure 8.2: Impulse (left) and magnitude responses (right) of the p-filters $\tilde{\mathbf{h}}^s$ and $\mathbf{h}^s$, $s = 2, 3$, derived from quadratic quasi-interpolating splines (non-interpolating low-pass p-filter)

Pseudo-spline: The FR of the non-interpolating low-pass p-filter $\mathbf{h}^0$ and the corresponding high-pass p-filter $\mathbf{h}^1$ are given by Eq. (7.18). We have

$$t[n]_1 \stackrel{\text{def}}{=} 1 - |h_0^0[n]_1|^2 - |h_1^0[n]_1|^2 = \frac{2(\omega^{2n} - 2 + \omega^{-2n})^2\, Q[n]_1}{256^2},$$
$$Q[n]_1 \stackrel{\text{def}}{=} -9\omega^{4n} - 28\omega^{2n} + 1610 - 28\omega^{-2n} - 9\omega^{-4n}.$$

1. Non-symmetric factorization $t[n]_1 = A[n]_1\, A[-n]_1$:

$$A[n]_1 = \frac{3(\omega - 2 + \omega^{-1})(1 - \alpha_1\omega^{2n})(1 + \alpha_2\omega^{2n})}{256\sqrt{\alpha_1\,\alpha_2}} \tag{8.10}$$
$$\alpha_1 = 0.084036721311635863751390197446785, \quad \alpha_2 = 0.066541718952892961207287011854059.$$

   The FR of the p-filters $\mathbf{h}^2$ and $\mathbf{h}^3$ are defined in Eq. (8.1) with $\tilde{A}[n]_1 = A[n]_1$. The p-filter bank $\mathbf{H} = \{\mathbf{h}^s\}$, $s = 0, 1, 2, 3$, generates a tight frame. The framelet $\psi^1_{[1]}$ has four LDVM, while $\psi^2_{[1]}$ and $\psi^3_{[1]}$ have two. The IR of the p-filters $\mathbf{h}^s$, $s = 0, 1, 2, 3$, and their MR are displayed in Fig. 8.7 (center).

2. Symmetric factorization $t[n]_1 = A[n]_1\, \tilde{A}[-n]_1$:

$$A[n]_1 = \frac{\sqrt{2}(-\omega^{2n} + 2 - \omega^{-2n})^2\, Q[n]_1}{8192}, \quad \tilde{A}[n]_1 = \frac{\sqrt{2}(-\omega^{2n} + 2 - \omega^{-2n})^2}{4}. \tag{8.11}$$

   The FR of the p-filters $\tilde{\mathbf{h}}^s$ and $\mathbf{h}^s$, $s = 2, 3$, are defined in Eq. (8.1). The p-filters $\mathbf{h^s}$ and $\tilde{\mathbf{h}}^s, : s = 2, 3$, locally eliminate sampled polynomials of first degree, thus the framelets $\psi^2_{[1]}$ and $\psi^s_{[1]}$ have two LDVM.

3. Antisymmetric factorization of $t[n]_1 = A[n]_1\, \tilde{A}[-n]_1$, which assigns three LDVM to the analysis framelet $\tilde{\psi}^2_{[1]}$ leaving only one LDVM to the synthesis framelet $\psi^2_{[1]}$ and vice versa for the framelets $\tilde{\psi}^3_{[1]}$ and $\psi^3_{[1]}$:

$$\tilde{A}[n]_1 = \sqrt{2}\,\frac{\omega^{4n} - 3\omega^{2n} + 3 - \omega^{-2n}}{8}, \quad A[n]_1 = \sqrt{2}\,\frac{\left(1 - \omega^{2n}\right)\, Q[n]_1}{4096}. \tag{8.12}$$

   The FR of the p-filters $\tilde{\mathbf{h}}^s$ and $\mathbf{h}^s$, $s = 2, 3$, are defined in Eq. (8.1). Figure 8.3 displays the IR of the p-filters $\mathbf{h}^s$, which are the discrete time framelets of the first level, and their MR.

Figure 8.3: Impulse (left) and magnitude responses (right) of the p-filters $\tilde{\mathbf{h}}^s$ and $\mathbf{h}^s$, $s = 2, 3$, derived from the pseudo-spline

8.2 Four-channel p-filter banks with p-IIR p-filters

Unlike non-periodic setting, implementation cost of IIR p-filters is no higher than the cost of p-FIR p-filters. However, giving up the requirement of finite impulse response provides additional flexibility in the design of p-filter banks with necessary properties. For the design, we use the prediction p-filters derived from the interpolating splines, which were described in Section 7

Quadratic interpolating spline $p = 3$: Denote $\Omega_c^3[n]_1 \stackrel{\text{def}}{=} \omega^{2n} + 6 + \omega^{-2n}$. The prediction p-filter $\mathbf{f}_c^3$ and the p-filters $\mathbf{h}^0$ and $\mathbf{h}^1$ are defined in Eq. (7.7). The p-filter $\mathbf{h}^0$ locally restores the sampled cubic polynomials while the p-filter $\mathbf{h}^1$ locally eliminates them. Thus, the framelet $\psi_{[1]}^1$ has four LDVM. We have $W[n]_1 = \left(\omega^{2n} - 2 + \omega^{-2n}/\Omega_c^3[n]_1\right)^2$.

1. Symmetric factorization $W[n]_1/2 = A[n]_1\, A[-n]_1$, , where

$$A[n]_1 = \frac{(\omega^{-2n} - 2 + \omega^{2n})}{\Omega_c^3[n]_1}. \tag{8.13}$$

   The FR of the p-filters $\mathbf{h}^2$ and $\mathbf{h}^3$ are defined in Eq. (8.1) where $\tilde{A}[n]_1 = A[n]_1$. The p-filter bank $\mathbf{H} = \{\mathbf{h}^s\}$, $s = 0, 1, 2, 3$, generates a tight frame. The framelets $\psi_{[1]}^s$, $s = 2, 3$, have two LDVM. The IR of the p-filters $\mathbf{h}^s$, $s = 0, 1, 2, 3$, and their MR are displayed in Fig. 8.7 (third from bottom).

2. Antisymmetric factorization of $W[n]_1 = A[n]_1\, \tilde{A}[-n]_1$, which assigns three LDVM to the analysis framelets $\widetilde{\psi_{[1]}^s}$ leaving only one LDVM to the synthesis framelets $\psi_{[1]}^s$, $s = 2, 3$:

$$\tilde{A}[n]_1 = \frac{\omega^{4n} - 3\omega^{2n} + 3 - \omega^{-2n}}{2\Omega_c^3[n]_1}, \quad A[n]_1 = \frac{2\left(1 - \omega^{2n}\right)}{\Omega_c^3[n]_1}. \tag{8.14}$$

   The FR of the p-filters $\tilde{\mathbf{h}}^s$ and $\mathbf{h}^s$, $s = 2, 3$, are defined in Eq. (8.1). Figure 8.4 displays the IR of the p-filters $\tilde{\mathbf{h}}^s$ and $\mathbf{h}^s$, $s = 2, 3$, which are the discrete time framelets of the first level, and their MR.

Figure 8.4: Impulse (left) and magnitude responses (right) of the p-filters $\tilde{\mathbf{h}}^s$ and $\mathbf{h}^s$, $s = 2, 3$, derived from quadratic interpolating spline

Cubic interpolating spline: $p = 4$: Denote

$$\Omega_c^4[n]_1 \stackrel{\text{def}}{=} \omega^{2n} + 4 + \omega^{-2n}, \quad \Gamma_c^4[n]_1 \stackrel{\text{def}}{=} -\omega^{2n} + 14 - \omega^{-2n}. \tag{8.15}$$

The prediction p-filter $\mathbf{f}_c^4$ and the p-filters $\mathbf{h}^0$ and $\mathbf{h}^1$ are defined in Eq. (7.8). The p-filter $\mathbf{h}^0$ locally restores the sampled cubic polynomials while the p-filter $\mathbf{h}^1$ locally eliminates them. Thus, the framelet $\psi_{[1]}^1$ has four LDVM. We have

$$W[n]_1 = \left(\frac{\omega^{2n} - 2 + \omega^{-2n}}{8\Omega_c^4[n]_1}\right)^2 \Gamma_c^4[n]_1. \tag{8.16}$$

Comparing Eq. (8.21) with Eq. (8.3), we observe that the numerators of the sequences $W[n]_1$ in both cases is the same. Therefore, factorization of $W[n]_1$ for the cubic interpolating spline is similar to the factorization for the quadratic quasi-interpolating spline.

1. Non-symmetric factorization $W[n]_1 = A[n]_1\, A[-n]_1$, where

$$A[n]_1 = \frac{\omega^{2n} - 2 + \omega^{-2n}}{8\sqrt{q}\,\Omega_c^4[n]_1}\left(1 - q\omega^{2n}\right), \quad q = 7 - 4\sqrt{3}. \tag{8.17}$$

   The FR of the p-filters $\mathbf{h}^2$ and $\mathbf{h}^3$ are defined in Eq. (8.1) where $\tilde{A}[n]_1 = A[n]_1$. The p-filter bank $\mathbf{H} = \{\mathbf{h}^s\}$, $s = 0, 1, 2, 3$, generates a tight frame. The framelets $\psi^s_{[1]}$, $s = 2, 3$, have two LDVM. The IR of the p-filters $\mathbf{h}^s$, $s = 0, 1, 2, 3$, and their MR are displayed in Fig. 8.7 (second from bottom).

2. Symmetric factorization $W[n]_1 = A[n]_1\, \tilde{A}[-n]_1$, where

$$\tilde{A}[n]_1 = \frac{\omega^{2n} - 2 + \omega^{-2n}}{8\,\Omega_c^4[n]_1}, \quad A[n]_1 = \tilde{A}[n]_1\, \Gamma_c^4[n]_1. \tag{8.18}$$

   The p-filters $\mathbf{h^s}$ and $\tilde{\mathbf{h}}^s$,: $s = 2, 3$, locally eliminate sampled polynomials of first degree, thus the framelets $\psi^2_{[1]}$ and $\psi^s_{[1]}$ have two LDVM.

3. Antisymmetric factorization $W[n]_1 = A[n]_1\, \tilde{A}[-n]_1$, which assigns three LDVM to the analysis $\tilde{\psi^2}_{[1]}$ and one LDVM to the synthesis $\psi^2_{[1]}$ framelets and vice versa for $\tilde{\psi^3}_{[1]}$ and one LDVM in synthesis $\psi^3_{[1]}$:

$$\tilde{A}[n]_1 = \frac{\omega^{4n} - 3\omega^{2n} + 3 - \omega^{-2n}}{4\,\Omega_c^4[n]_1}, \quad A[n]_1 = \frac{\left(1 - \omega^{2n}\right)\,\Gamma_c^4[n]_1}{16\,\Omega_c^4[n]_1}. \tag{8.19}$$

   The FR of the p-filters $\tilde{\mathbf{h}}^s$ and $\mathbf{h}^s$, $s = 2, 3$, are defined in Eq. (8.1). Figure 8.5 displays the IR of the p-filters $\tilde{\mathbf{h}}^s$ and $\mathbf{h}^s$, $s = 2, 3$, which are the discrete time framelets of the first level, and their MR.

Figure 8.5 displays the IR of the p-filters $\tilde{\mathbf{h}}^s$ and $\mathbf{h}^s$, $s = 2, 3$, which are the discrete time framelets of the first level, and their MR. The IR of the p-filters $\mathbf{h}^2$ and $\mathbf{h}^3$ are nonsymmetric. Their magnitude responses are equal to each other but their phase responses are different. The same is true for $\tilde{\mathbf{h}}^2$ and $\tilde{\mathbf{h}}^3$.

Figure 8.5: Impulse (left) and magnitude responses (right) of the p-filters $\tilde{\mathbf{h}}^s$ and $\mathbf{h}^s$, $s = 2, 3$, derived from cubic interpolating spline

Interpolating spline of fourth degree, $p = 5$: Denote

$$\Omega_c^5[n]_1 \stackrel{\text{def}}{=} \omega^{4n} + 76\omega^{2n} + 230 + 76\omega^{-2n} + \omega^{-4n}, \quad \Gamma_c^5[n]_1 \stackrel{\text{def}}{=} -\omega^{2n} + 98 - \omega^{-2n}. \tag{8.20}$$

Then,

$$f_c^5[n]_1 = 16\,\frac{\omega^{4n} + 11\omega^{2n} + 11 + \omega^{-2n}}{\Omega_c^5[n]_1}, \quad W[n]_1 = \left(-\omega^{2n} + 2 - \omega^{-2n}\right)^3\,\frac{\Gamma_c^5[n]_1}{\left(\Omega_c^5[n]_1\right)^2}, \tag{8.21}$$

$$\hat{h}^0[n] = \sqrt{2}\,128\,\frac{\cos^6 \pi n/N\,(2 + \cos^2 \pi n/N)}{\Omega_c^5[n]_1}, \quad \hat{h}^1[n] = \sqrt{2}\,128\,\frac{\sin^6 \pi n/N\,(2 + \sin^2 \pi n/N)}{\Omega_c^5[n]_1}.$$

The p-filter $\mathbf{h}^0$ locally restores the sampled polynomials of the fifth degree while the p-filter $\mathbf{h}^1$ locally eliminates them. Thus, the framelet $\psi^1_{[1]}$ has six LDVM.

1. Non-symmetric factorization $W[n]_1 = A[n]_1\, A[-n]_1$, where

$$A[n]_1 = \frac{\omega^{2n} - 3 + 3\omega^{-2n} - \omega^{-4n}}{\sqrt{q}\,\Omega_c^5[n]_1}\left(1 - q\omega^{2n}\right), \quad q = 49 - 20\sqrt{6}. \tag{8.22}$$

   The FR of the p-filters $\mathbf{h}^2$ and $\mathbf{h}^3$ are defined in Eq. (8.1) with $\tilde{A}[n]_1 = A[n]_1$. The p-filter bank $\mathbf{H} = \{\mathbf{h}^s\}$, $s = 0, 1, 2, 3$, generates a tight frame. The framelets $\psi^2_{[1]}$ and $\psi^3_{[1]}$ have three LDVM. The IR of the p-filters $\mathbf{h}^s$, $s = 0, 1, 2, 3$, and their MR are displayed in Fig. 8.7 (bottom).

2. Symmetric factorization $W[n]_1 = A[n]_1\, \tilde{A}[-n]_1$, which assigns four LDVM to the analysis $\tilde{\psi}^s_{[1]}$ and two LDVM to the synthesis $\psi^s_{[1]}$, $s = 2, 3$, framelets:

$$A[n]_1 = -\frac{\omega^{2n} - 2 + \omega^{-2n}}{8\sqrt{2}\,\Omega_c^5[n]_1}\,\Gamma_c^5[n]_1, \quad \tilde{A}[n]_1 = 8\sqrt{2}\,\frac{\left(\omega^{2n} - 2 + \omega^{-2n}\right)^2}{\Omega_c^5[n]_1}. \tag{8.23}$$

3. Antisymmetric factorization $W[n]_1 = A[n]_1\, \tilde{A}[-n]_1$:

$$\tilde{A}[n]_1 = \frac{\omega^{2n} - 3 + 3\omega^{-2n} - \omega^{-4n}}{8\sqrt{2}\;\Omega_c^5[n]_1}, \quad A[n]_1 = \tilde{A}[n]_1\,\frac{\Gamma_c^5[n]_1}{128}. \tag{8.24}$$

Figure 8.6 displays the IR of the p-filters $\tilde{\mathbf{h}}^s$ and $\mathbf{h}^s$, $s = 2, 3$, which are the discrete time framelets of the first level, and their magnitude responses.

Figure 8.6: Impulse (left) and magnitude responses (right) of the p-filters $\tilde{\mathbf{h}}^s$ and $\mathbf{h}^s$, $s = 2, 3$, derived from interpolating spline of fifth order (fourth degree)

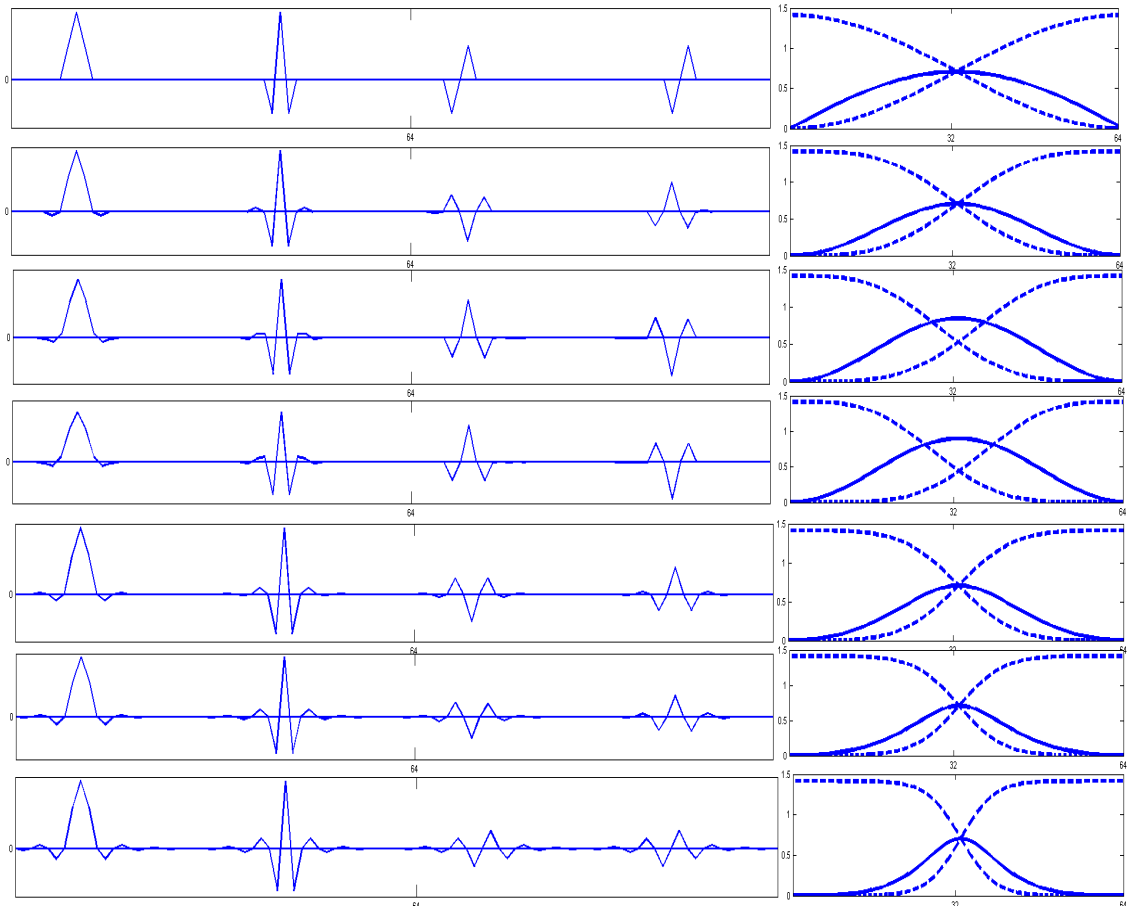

Figure 8.7: Impulse and magnitude responses of the IIR p-filter banks that generate tight frames. Left pictures display the IR of the p-filters. Left to right: $\mathbf{h}^0 \longrightarrow \mathbf{h}^1 \longrightarrow \mathbf{h}^2 \longrightarrow \mathbf{h}^3$. Right pictures display the MR of these p-filters: $\mathbf{h}^0$ and $\mathbf{h}^1$ (dashed lines), $\mathbf{h}^3$ and $\mathbf{h}^2$, whose MR coincide with each other (solid line). From top to bottom, the p-filters derived from: linear spline, quadratic quasi-interpolating spline (interpolating low-pass p-filter)), quadratic quasi-interpolating spline(non-interpolating low-pass p-filter)), pseudo-spline, quadratic interpolating spline, cubic interpolating spline and interpolating spline of order 5

9 Application of periodic frames to image restoration

In this section, we present the results from the application of the developed framelets to image restoration. The images were degraded by blurring aggravated by random noise and by random loss of significant number of pixels. The images are transformed by periodic frames designed in Section 8, which are extended to the 2D setting in a standard tensor product way. The goal of our experiments is to compare between the performances of different tight and semi-tight frames in identical conditions.

9.1 Outline of the restoration scheme

The images are restored by the application of the *split Bregman iteration* (SBI) scheme [16] that uses the so-called analysis based approach (see for example [19]).

Denote by $\mathbf{u} = \{u[\kappa, \nu]\}$ the original image array to be restored from the degraded array $\mathbf{f} = \mathbf{K}\,\mathbf{u} + \varepsilon$, where $\mathbf{K}$ denotes the 2D discrete convolution operator of the array $\mathbf{u}$ with a kernel $\mathbf{k} = \{k[\kappa, \nu]\}$ and

$\varepsilon = \{e_{k,n}\}$ is the random error array. $\bar{\mathbf{K}}$ denotes the conjugate operator of $\mathbf{K}$, which implements the discrete convolution with the transposed kernel $\mathbf{k}^T$. If some number of pixels are missing then the image $\mathbf{u}$ should be restored from the available data

$$\mathbf{P_\Lambda}\,\mathbf{f} = \mathbf{P_\Lambda}\,(\mathbf{K}\,\mathbf{u} + \varepsilon), \tag{9.1}$$

where the symbol $\mathbf{P_\Lambda}$ denotes the projection on the remaining pixels set.

The solution scheme is based on the assumption that the original image $\mathbf{u}$ has a sparse representation in a frame domain. Denote by $\tilde{\mathbf{F}}$ the frame expansion operator of the image $\mathbf{u}$ where $\mathbf{C} \stackrel{\text{def}}{=} \tilde{\mathbf{F}}\,\mathbf{u}$, $\mathbf{C} = \{c[\kappa,\nu]\}$, is the frame coefficients set. Denote by $\mathbf{F}$ the reconstruction operator for the image $\mathbf{u}$ from the set of the frame coefficients. We get $\mathbf{F}\,\mathbf{C} = \mathbf{u}$, $\mathbf{F}\,\tilde{\mathbf{F}} = \mathbf{I}$, where $\mathbf{I}$ is the identity operator.

We assumed that the approximated solution to Eq. (9.1) is derived via minimization of the functional

$$\min_u \frac{1}{2}\,\|\mathbf{P_\Lambda}\,(\mathbf{K}\,\mathbf{u} - f)\|_2^2 + \lambda\,\|\tilde{\mathbf{F}}\,\mathbf{u}\|_1, \tag{9.2}$$

where $\|\cdot\|_1$ and $\|\cdot\|_2$ are the l_1 and l_2 norms of the sequences, respectively. If $\mathbf{x} = \{x[\kappa,\nu]\}\,,\ \kappa = 0,...,k,\ \nu = 0,...,n$, then

$$\|\mathbf{x}\|_1 \stackrel{\text{def}}{=} \sum_{\kappa=0}^{k-1}\sum_{\nu=0}^{n-1} |x[\kappa,\nu]|, \quad \|\mathbf{x}\|_2 \stackrel{\text{def}}{=} \sqrt{\sum_{\kappa=0}^{k-1}\sum_{\nu=0}^{n-1} |x[\kappa,\nu]|^2}.$$

Denote by $\mathbf{T}_\vartheta$ the operator of soft thresholding:

$$\mathbf{T}_\vartheta\,\mathbf{x} = \{x_\vartheta[\kappa,\nu]\}\,, \quad x_\vartheta[\kappa,\nu] \stackrel{\text{def}}{=} \operatorname{sgn}(x[\kappa,\nu])\,\max\{0, |x[\kappa,\nu]| - \vartheta\}\,.$$

Following [19], we solve the minimization problem in Eq. (9.2) by an iterative algorithm. We begin with the initialization $\mathbf{u}^0 = 0,\ \mathbf{d}^0 = \mathbf{b}^0 = 0$. Then,

$$\begin{aligned}
&\mathbf{u}^{k+1} := (\bar{\mathbf{K}}\,\mathbf{P_\Lambda}\,\mathbf{K} + \mu\,\mathbf{I})\,\mathbf{u} = \bar{\mathbf{K}}\,\mathbf{P_\Lambda}\,\mathbf{f} + \mu\,\mathbf{F}\,(\mathbf{d}^k - \mathbf{b}^k),\\
&\mathbf{d}^{k+1} = \mathbf{T}_{\lambda/\mu}(\tilde{\mathbf{F}}\,\mathbf{u}^{k+1} + \mathbf{b}^k),\\
&\mathbf{b}^{k+1} = \mathbf{b}^k + (\tilde{\mathbf{F}}\,\mathbf{u}^{k+1} - \mathbf{d}^{k+1}).
\end{aligned} \tag{9.3}$$

The linear system in the first line of Eq. (9.3) is solved by the application of the *conjugate gradient* algorithm. The operations in the second and third lines are straightforward. The choice of the parameters λ and μ depends on experimental conditions.

9.2 Experimental results

The restoration algorithms were applied to "Window", "Barbara", "Boats", "Lena" and "Fingerprint" images. These images were blurred by convolution with the motion or with the Gaussian kernel and degraded by the fact that a large number of pixels were missing. In some experiments, the degradation was aggravated by addition of zero mean random noise.

In the experiments, we compare between the performance of tight frames (TF) and semi-tight frames (STF). The framelets in table 2 participated in the experiments and they are denoted by the following notation:

$\mathbf{T}^1$	LS TF, Eqs. (7.6),(8.2),		$\mathbf{S}_1^4$	PS STF, Eqs. (7.18),(8.12),
$\mathbf{T}^2$	QqSi TF, Eqs. (7.14),(8.4),		$\mathbf{T}^5$	QIS TF, Eqs. (7.7),(8.13),
$\mathbf{S}_1^2$	QqSi STF, Eqs. (7.14),(8.5),		$\mathbf{T}_1^5$	QIS STF, Eqs. (7.7),(8.14),
$\mathbf{S}_2^2$	QqSi STF, Eqs. (7.14),(8.6),		$\mathbf{T}^6$	CIS TF, Eqs. (7.8), (8.17),
$\mathbf{T}^3$	QqSn TF, Eqs, (7.13),(8.7),		$\mathbf{S}_1^6$	CIS STF, Eqs. (7.8), (8.18),
$\mathbf{S}_1^3$	QqSn STF, Eqs. (7.13), (8.8)		$\mathbf{S}_2^6$	CIS STF, Eqs. (7.8), (8.19),
$\mathbf{S}_2^2$	QqSn STF, Eqs. (7.13),(8.9),		$\mathbf{T}^7$	IS5 TF, Eqs. (8.21), (8.22),
$\mathbf{T}^4$	PS SF, Eqs. (7.18), (8.10),		$\mathbf{S}_1^7$	IS5 STF, Eqs. (8.21), (8.23)
$\mathbf{S}_1^4$	PS STF, Eqs. (7.18), (8.11),		$\mathbf{S}_2^7$	IS5 STF, Eqs. (8.21),(8.23).

Table 2: Four-channel p-filter banks. LS – linear spline, QIS – quadratic interpolating spline, QqSi – quadratic quasi-interpolating spline (interpolating low-pass p-filter), QqSn – quadratic quasi-interpolating spline (non-interpolating low-pass p-filter), CIS – cubic interpolating spline, PS – pseudo-spline, IS5– interpolating spline of order 5.

The proximity between an image $\tilde{\mathbf{u}}$ and the original image $\mathbf{u}$ is evaluated visually and by the Peak-Signal-to-Noise ratio (PSNR)

$$PSNR \stackrel{\text{def}}{=} 10 \log_{10} \left(\frac{M\, 255^2}{\sum_{k=1}^{M} (x_k - \tilde{x}_k)^2} \right) \, dB. \tag{9.4}$$

where M is the number of pixels in the image (in our experiments, $M = 512^2$), $\{x_k\}_{k=1}^M$ are the original pixels of the image $\mathbf{u}$ and $\{\tilde{x}_k\}_{k=1}^M$ are the pixels of the image $\tilde{\mathbf{u}}$.

Restoration experiments for the "Window" image This image was taken from [19]. The image was blurred by convolution with the motion kernel (MATLAB function `fspecial`('motion',15,45)) and its PSNR becomes 23.56 dB. Then, 30% of pixels were randomly removed. This reduces the PSNR to 10,22 dB. No random noise was added. The image was restored by 50 SBI using the parameters $\lambda = 0.001$, $\mu = 0.001$ in Eq. (9.3). The conjugate gradient solver used 100 iterations. The tight and semi-tight frames listed in Table 2 were tested. The decomposition is implemented down to the fifth level. The restored PSNR results are given in Table 3.

Frame	$\mathbf{T}^1$	$\mathbf{T}^2$	$\mathbf{S}_1^2$	$\mathbf{S}_2^2$	$\mathbf{T}^3$	$\mathbf{S}_1^3$	$\mathbf{S}_2^3$	$\mathbf{T}^4$	$\mathbf{S}_1^4$
PSNR	42.36	43.13	43.15	43.22	43.54	**43.78**	43.63	43.74	43.65
Frame	$\mathbf{S}_2^4$	$\mathbf{T}^5$	$\mathbf{S}_1^5$	$\mathbf{T}^6$	$\mathbf{S}_1^6$	$\mathbf{S}_2^6$	$\mathbf{T}^7$	$\mathbf{S}_1^7$	$\mathbf{S}_2^7$
PSNR	**43.78**	43.20	43.04	43.12	43.14	42.89	42.83	42.84	42.79

Table 3: PSNR results after the restoration of the "Window" image that was a blurred input where of 30% of its pixels were randomly removed

The best PSNR results (43.78 dB) is achieved by using the four-channel semi-tight frames $\mathbf{S}_1^3$ and $\mathbf{S}_2^4$ derived from the quadratic quasi-interpolating spline (non-interpolating low-pass p-filter) and the pseudo-spline, respectively. The frame $\mathbf{S}_1^3$ results from the symmetric factorization of the sequence $t[n]_1$ in Eq. (8.8), which provides two LDVM to either of the framelets $\tilde{\psi}_{[1]}^s$ and $\psi_{[1]}^s$, $s = 2, 3$. The frame $\mathbf{S}_2^4$ results from the antisymmetric factorization of $t[n]_1 = A[n]_1 \, \tilde{A}[-n]_1$, which assigns three LDVM to the analysis framelet $\tilde{\psi}_{[1]}^2$ leaving only one LDVM to the synthesis framelet $\psi_{[1]}^2$ and vice versa for the framelets $\tilde{\psi}_{[1]}^3$ and $\psi_{[1]}^3$.

Figure 9.1 displays the restoration result. Visually, the restored image hardly can be distinguished from the original one.

Figure 9.1: Top left: Source input - "Window" image. Top right: Blurred. PSNR=23.56 dB. Bottom right: After random removal of 30% of its pixels. PSNR=10.22 dB. Bottom left: The best restored image was achieved by the frame $\mathbf{S}_1^3$. PSNR=43.78 dB

Results from the restoration of the "Boats" image: The SBI algorithm, which uses the spline-based frames, was able to restore images even when most of the pixels were missing. It is demonstrated on the restoration of the "Boats" image. The image was blurred by convolution with the motion kernel (MATLAB function `fspecial`('motion',15,45)) and its PSNR becomes 22.88 dB. Then, 70% of pixels were randomly removed. This reduces the PSNR to 7.37 dB. Random noise was not added. The image was restored by 50 SBI using the parameters $\lambda = 0.025,\ \mu = 0.001$ in Eq. (9.3). The conjugate gradient solver used 30 iterations. The tight and semi-tight frames listed in Table 2 were tested. The decomposition was implemented only one level down. The restored PSNR results are given in Table 4.

Frame	$\mathbf{T}^1$	$\mathbf{T}^2$	$\mathbf{S}_1^2$	$\mathbf{S}_2^2$	$\mathbf{T}^3$	$\mathbf{S}_1^3$	$\mathbf{S}_2^3$	$\mathbf{T}^4$	$\mathbf{S}_1^4$
PSNR	30.03	29.98	29.99	30.11	30.08	30.11	30.26	30.11	30.08
Frame	$\mathbf{S}_2^4$	$\mathbf{T}^5$	$\mathbf{S}_1^5$	$\mathbf{T}^6$	$\mathbf{S}_1^6$	$\mathbf{S}_2^6$	$\mathbf{T}^7$	$\mathbf{S}_1^7$	$\mathbf{S}_2^7$
PSNR	**30.28**	29.86	29.76	29.66	29.66	29.68	29.26	29.26	29.25

Table 4: PSNR results after the restoration of the "Boats" image that was blurred and 70% of its pixels were randomly removed

As in previous experiments, the best PSNR results 30.28 dB was achieved by the application of the four-channel semi-tight frame $\mathbf{S}_2^4$ derived from the pseudo-spline using anti-symmetric factorization. This result is displayed in Fig. 9.2. The decomposition is implemented to the second level. The used parameters are $\lambda = 0.006$ and $\mu = 0.001$ in Eq. (9.3).

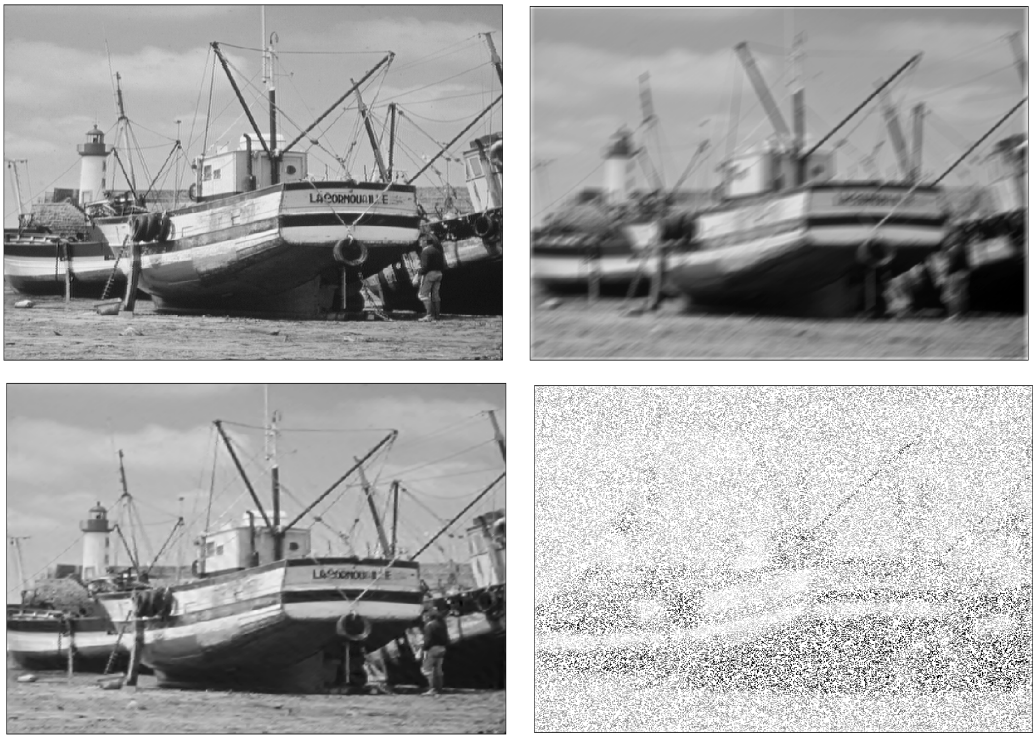

Figure 9.2: Top left: Source input - "Boats" image. Top right: Blurred. PSNR=22.88 dB. Bottom right: After random removal of 70% from its pixels. PSNR=7.37 dB. Bottom left: The best restored image was produced by the frame $\mathbf{S}_2^4$. PSNR=30.28 dB

Results from the restoration of the "Barbara" image: In these experiments, the "Barbara" image was restored after it was blurred by a convolution with the Gaussian kernel (MATLAB function `fspecial`('gaussian',[5 5],5)) and its PSNR became 23.06 dB. Then, 50% of its pixels were randomly removed. This reduces the PSNR to 7.55 dB. Random noise was not added. The image was restored by 50 SBI using the parameters $\lambda = 0.001$, $\mu = 0.001$ in Eq. (9.3). The conjugate gradient solver used 70 iterations. Tight and semi-tight frames listed in Table 2 were tested. The decomposition is implemented down to the second level. The restored PSNR results are given in Table 5.

Frame	$\mathbf{T}^1$	$\mathbf{T}^2$	$\mathbf{S}_1^2$	$\mathbf{S}_2^2$	$\mathbf{T}^3$	$\mathbf{S}_1^3$	$\mathbf{S}_2^3$	$\mathbf{T}^4$	$\mathbf{S}_1^4$
PSNR	29.14	29.56	29.57	29.55	29.68	29.74	29.68	29.73	29.72
Frame	$\mathbf{S}_2^4$	$\mathbf{T}^5$	$\mathbf{S}_1^5$	$\mathbf{T}^6$	$\mathbf{S}_1^6$	$\mathbf{S}_2^6$	$\mathbf{T}^7$	$\mathbf{S}_1^7$	$\mathbf{S}_2^7$
PSNR	29.71	29.79	29.79	29.95	29.95	29.91	**30.114**	30.106	30.111

Table 5: PSNR results after the restoration of the "Barbara" image that was blurred and then 50% of its pixels were randomly removed

PSNR of 30.11 dB was the best. It was achieved by application of the four-channel tight frame $\mathbf{T}^7$ derived from the interpolating spline of the fifth order although the semi-tight frames $\mathbf{S}_1^7$ and $\mathbf{S}_2^7$ performed similarly. The p-filters used in these frames have maximal number of LDVM compared to other frames listed in in Table 2. The restoration result from the application of the frame $\mathbf{T}^7$ is displayed in Fig. 9.3. We observe that fine texture of the image, which is undistinguishable in the blurred image, is restored accurately.

Figure 9.3: Top left: Source input - "Barbara" image. Top right: Blurred and noised. PSNR=23.20 dB. Bottom right: After random removal of 30% of its pixels. PSNR=10.2 dB. Bottom left: The restored image by application of the frame $\mathbf{S}_7^4$. PSNR=28.76 dB

Results from the restoration of the "Lena" image: The source image was strongly burred by convolution with a Gaussian kernel (MATLAB function `fspecial`('gaussian',[12,12],12)) (PSNR=23.44 dB). The blurred image is distorted by randomly drawn curves (PSNR=16.37 dB). Noise was not added. The image is restored by 50 SBI with the parameters $\lambda = 0.09$ and $\mu = 0.17$ by the four-channel frames listed in Table 2. The decomposition was implemented down to the fifth level. The conjugate gradient solver used 11 iterations. The PSNR results are given in Table 6.

Frame	$\mathbf{T}^1$	$\mathbf{T}^2$	$\mathbf{S}_1^2$	$\mathbf{S}_2^2$	$\mathbf{T}^3$	$\mathbf{S}_1^3$	$\mathbf{S}_2^3$	$\mathbf{T}^4$	$\mathbf{S}_1^4$
PSNR	28.77	28.72	28.73	28.86	28.77	28.85	**28.90**	28.79	28.78
Frame	$\mathbf{S}_2^4$	$\mathbf{T}^5$	$\mathbf{S}_1^5$	$\mathbf{T}^6$	$\mathbf{S}_1^6$	$\mathbf{S}_2^6$	$\mathbf{T}^7$	$\mathbf{S}_1^7$	$\mathbf{S}_2^7$
PSNR	28.88	28.76	28.60	28.73	28.75	28.76	28.63	28.646	28.65

Table 6: PSNR results after the restoration of the "Barbara" image that was a blurred and 50% of its pixels were randomly removed

PSNR result of 28.90 dB was the best. It was achieved by the application of the four-channel semi-tight frames $\mathbf{S}_2^3$ and $\mathbf{S}_2^4$ derived from the quadratic quasi-interpolating spline (non-interpolating low-pass p-filter) and the pseudo-spline, respectively. These frames result from the antisymmetric factorization of $t[n]_1 = A[n]_1\,\tilde{A}[-n]_1$, which assigns three LDVM to the analysis framelet $\widetilde{\psi_{[1]}^2}$ leaving only one LDVM to the synthesis framelet $\psi_{[1]}^2$ and vice versa for the framelets $\tilde{\psi}_{[1]}^3$ and $\psi_{[1]}^3$. Figure 9.4 displays the best restoration

result. We observe that the corrupting curves are completely removed and the image is deblurred.

Figure 9.4: Top left: Source input - "Lena" image. Top right: Blurred. PSNR=23.44 dB. Bottom right: Distorted by randomly drawn curves. PSNR=16.37 dB. Bottom left: The restored image by the application of the semi-tight frame $\mathbf{S}_6^3$. PSNR=28.90 dB

Results from the restoration of the "Fingerprint" image: Unlike previous experiments, the "Fingerprint" image was affected by a strong zero-mean white noise with STD $\sigma = 20$ after being blurred by convolution with the Gaussian kernel (MATLAB function `fspecial`('gaussian',[5 5],5)) (PSNR=19.75 dB). Then, 50% of its pixels were randomly removed and this produced PSNR=9.05 dB. The image was restored by 50 SBI with the parameters $\lambda = 2.3$ and $\mu = 0.45$ using the tight and semi-tight frames listed in Table 2. The decomposition is implemented down to the fifth level. The conjugate gradient solver used 12 iterations. The PSNR results are given in Table 7.

Frame	$\mathbf{T}^1$	$\mathbf{T}^2$	$\mathbf{S}_1^2$	$\mathbf{S}_2^2$	$\mathbf{T}^3$	$\mathbf{S}_1^3$	$\mathbf{S}_2^3$	$\mathbf{T}^4$	$\mathbf{S}_1^4$
PSNR	22.38	23.11	23.12	23.25	23.14	23.26	23.22	23.15	23.13
Frame	$\mathbf{S}_2^4$	$\mathbf{T}^5$	$\mathbf{S}_1^5$	$\mathbf{T}^6$	$\mathbf{S}_1^6$	$\mathbf{S}_2^6$	$\mathbf{T}^7$	$\mathbf{S}_1^7$	$\mathbf{S}_2^7$
PSNR	23.20	23.41	23.32	23.59	23.58	23.54	**23.75**	23.746	23.73

Table 7: PSNR results after the restoration of the "Fingerprint" image that was blurred and 50% of its pixels were randomly removed

PSNR=23.75 dB was the best results achieved by the application of the four-channel tight frame $\mathbf{T}^7$ derived from the interpolating spline of fifth order. Similar results were produced by the application of the

semi-tight frames derived from the same spline. Note that, like in the experiments with "Barbara", the maximum PSNR results were achieved from frames that have the highest number of LDVM.

Figure 9.5 displays the restoration result produced by application of the $\mathbf{T}^7$ frame. Despite the strong noise and loss of a significant number of pixels,the structure of the image is effectively restored.

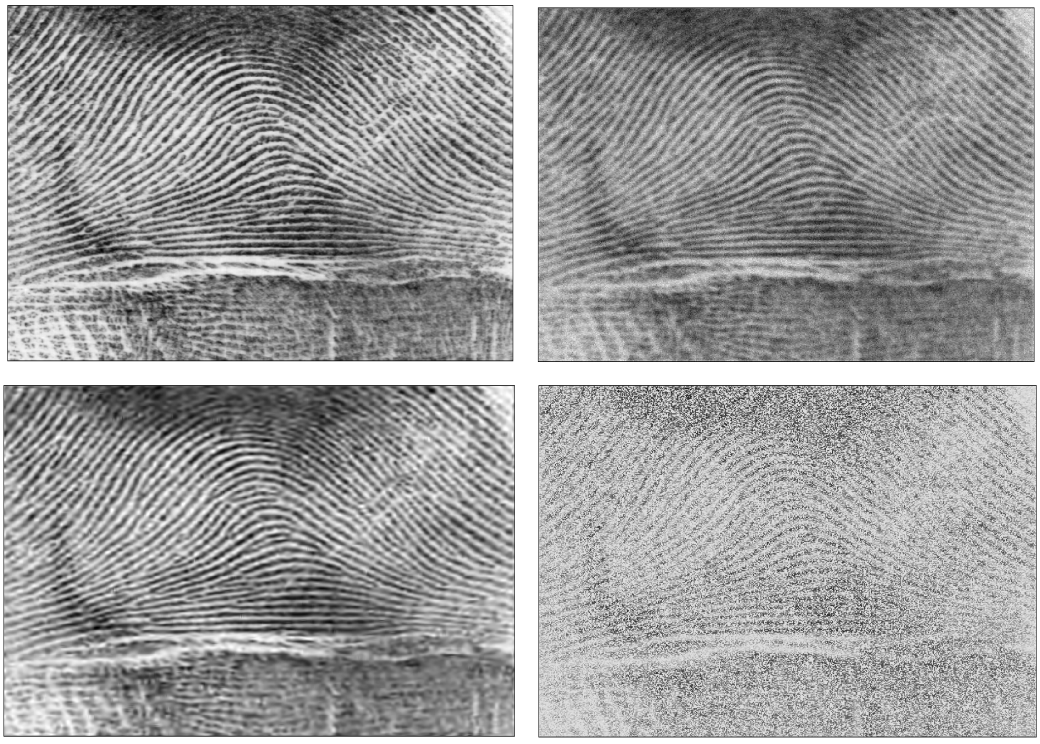

Figure 9.5: Top left: Source input - "Fingerprint" image. Top right: Blurred. PSNR=19.75 dB. Bottom right: After random removal of 50% of its pixels. PSNR=9.05 dB. Bottom left: The image was restored by the application of tight frame $\mathbf{T}^7$. PSNR=23.75 dB

9.2.1 Comments on the experiments

In the above experiments, the designed four-channel frames proved to be highly efficient for image restoration. It is important that the computational cost does not depend on the spline order. This makes the framelets with high number of LDVM and infinite impulse response suitable for utilization in implementation. In some cases, such as in the experiments with "Barbara" (Table 5) and "Fingerprint" (Table 7), the best results were produced by tight frames derived from interpolating spline of the fifth order, where the framelets $\psi^1_{[m]}$ have six LDVM and the framelets $\psi^2_{[m]}$ and $\psi^3_{[m]}$ have three of four LDVM and the interpolating low-pass p-filter locally restores polynomials of fifth degree. Note that both images have fine texture, which is satisfactorily restored after strong blurring, corrupting by noise ("Fingerprint") and then random removable of 50% of their pixels.

When image distortion is not strong, as in the "Window"image, it is restored close to perfection (Figs. 9.1). The images "Lena", which was strongly blurred, and "Boats", where 70 % of its pixels were missing, were successfully restored (Figs. 9.4 and 9.2). For these three images, which are relatively smooth, the best results were produced by the semi-tight frames, which are derived from the quasi-interpolating quadratic spline and the pseudo-spline. The low-pass p-filters in the generating p-filter banks are non-interpolating and have relatively long IR (9 taps). Note that in most cases, the semi-tight frames performed better than

their tight counterparts.

Typically, increase in the SBI number above 50 does not contribute into the restoration quality. In some cases, as in the "Window" and "Barbara" experiments, a big number of iterations of the conjugate gradient solver increased the restoration quality. However, in the experiments with the strongly degraded "Lena" and "Fingerprint" images, increase in the number of iterations above 12 depleted the quality.

Choice of the regularization parameters λ and μ is of crucial importance. The restoration quality is sensitive to them. Even a small change in the parameters significantly affects it. The number of decomposition levels is also important.

Conclusion and future work

We designed a library of tight and semi-tight wavelet frames (framelets) in the discrete-time periodic signals space, which are generated by four-channel perfect reconstruction periodic filter banks. The filter banks are derived from interpolating and quasi-interpolating polynomial splines. Since the common definition of vanishing moments is invalid in periodic setting, we introduce the notion of local discrete vanishing moments (LDVM). The design scheme is generic that makes it possible to design framelets with any number of LDVM.

The designed frames were tested for images restoration. These images were degraded by blurring, random noise and by random removal of many of their pixels. The images were restored by the application of the Split Bregman Iterations (SBI) method. The performances of the designed frames are compared. The designed frames proved to be very efficient for image restoration. The complexity of the computational scheme of the framelet transforms, which consists of forward inverse fast Fourier transforms computations added by simple arithmetical operations, is independent of the number of LDVM, size of the impulse response of the filters (up to infinite) and the number of decomposition levels. This property allows in each case to select the frame that best fits its task. For example, in the experiments with "Barbara" and "Fingerprint" images, the best performance was achieved by frames that were derived from the fifth order interpolating spline, where the high-frequency framelet has six LDVM and the low-pass p-filter is interpolating and locally restores polynomials of fifth degree. It happened that in most experiments the semi-tight frames outperformed their tight counterparts.

In a future work, we plan to modify the designed frames to process 3D images and apply them to processing seismic and hyper-spectral data. Another research direction is the design of periodic discrete-time multiwavelet frames, which is a continuation of the work started in [8].

References

[1] O. Amrani, A. Averbuch, T. Cohen, and V. A. Zheludev. Symmetric interpolatory framelets and their error correction properties. *International Journal of Wavelets, Multiresolution and Information Processing*, 5(4):541–566, 2007.

[2] A. Averbuch and V. Zheludev. Construction of biorthogonal discrete wavelet transforms using interpolatory splines. *Applied and Comp. Harmonic Analysis*, 12(12):25–56, 2002.

[3] A. Averbuch and V. Zheludev. Wavelet transforms generated by splines. *International Journal of Wavelets, Multiresolution and Information Processing*, 5(2):257–292, 2007.

[4] A. Z. Averbuch, A. B. Pevnyi, and V. A. Zheludev. Biorthogonal Butterworth wavelets derived from discrete interpolatory splines. *IEEE Trans. on Sign. Proc.*, 49:2682–2692, 2001.

[5] A. Z. Averbuch, A. B. Pevnyi, and V. A. Zheludev. Butterworth wavelet transforms derived from discrete interpolatory splines: Recursive implementation. *Signal Processing*, 81:2363–2382, 2001.

[6] A. Z. Averbuch, V. A. Zheludev, and T. Cohen. Interpolatory frames in signal space. *IEEE Trans. Sign. Proc.*, 54(6):2126–2139, June 2006.

[7] A. Z. Averbuch, V. A. Zheludev, and T. Cohen. Tight and sibling frames originated from discrete splines. *Sign. Proc. J.*, 86(7):1632–1647, 2006.

[8] A. Z. Averbuch, V. A. Zheludev, and T. Cohen. Multiwavelet frames in signal space originated from hermite splines. *IEEE Trans. on Signal Processing*, 55:797–808, 2007.

[9] B. Dong, Z. Shen. Pseudo-splines, wavelets and framelets. *Applied and Computational Harmonic Analysis*, 22(1):78–104, January 2007.

[10] H. Bölcskei, F. Hlawatsch, and H. G. Feichtinger. Frame-theoretic analysis of oversampled filter banks. *IEEE Transactions on Sign. Proc.*, 46(12):3256–3268, Dec 1998.

[11] C. K. Chui and W. He. Compactly supported tight frames associated with refinable functions. *Applied and Comp. Harmonic Analysis*, 8:293–319, 2000.

[12] C. K. Chui, W. He, and J. Stöckler. Compactly supported tight and sibling frames with maximum vanishing moments. *Applied and Comp. Harmonic Analysis*, 13:224–262, 2002.

[13] Z. Cvetković and M. Vetterli. Oversampled filter banks. *IEEE Transactions on Signal Processing*, 46(5):1245–1255, May 1998.

[14] I. Daubechies, Bin Han, A. Ron, and Z. Shen. Framelets: Mra-based constructions of wavelet frames. *Applied and Computational Harmonic Analysis*, 14(1–46), 2003.

[15] J. Romberg E. Candes and T. Tao. Stable signal recovery from incomplete and inaccurate measurements. *Communications on Pure and Applied Mathematics*, 59(8):1207–1223, 2006.

[16] T. Goldstein and S. Osher. The split Bregman method for l1-regularized problems. *SIAM J. Imaging Sciences*, 2(2):323–343, 2009.

[17] V. K Goyal, J. Kovacevic, and J.A. Kelner. Quantized frame expansions with erasures. *Appl. and Comput. Harmonic Analysis*, 10(3):203–233, 2001.

[18] V. K Goyal, M. Vetterli, and N. T. Thao. Quantized overcomplete expansions in $\mathbb{R}^n$: Analysis, synthesis and algorithms. *IEEE Trans. on Information Theory*, 44(1):16–31, 1998.

[19] Z. Shen H. Ji and Y. Xu. Wavelet frame based image restoration with missing/damaged pixels. *East Asia Journal on Applied Mathematics*, 1:108–131, 2011.

[20] S. Osher J. Cai, B. Dong and Z. Shen. Image restoration: total variation, wavelet frames, and beyond. *Journal of the American Mathematical Society*, 25:1033–1089, 2012.

[21] Z. Shen J. Cai, S. Osher. Split Bregman methods and frame based image restoration. *Multiscale Modeling and Simulation: A SIAM Interdisciplinary Journal*, 8(2):337–369, 2009.

[22] J. Kovacevic, P.L. Dragotti, and V. K Goyal. Filter bank frame expansions with erasures. *IEEE Trans. Inform*, 48(6):1439–1450, 2002.

[23] G. Polya and G. Szegö. *Aufgaben and Lehrsiitre aus der Analysis, Vol. II.* Springer, Berlin, 1971.

[24] B. Han S. Song Goh and Z. Shen. Tight periodic wavelet frames and approximation orders. *Applied and Computational Harmonic Analysis*, 31:228–248, 2011.

[25] I. J. Schoenberg. Contribution to the problem of approximation of equidistant data by analytic functions. *Quart. Appl. Math.*, 4:45–99, 112–141, 1946.

[26] Z. Shen. Wavelet frames and image restorations. In *Proc. Int. Congress of Mathematicians, vol. IV, Rajendra Bhatia eds.*, pages 2834–2863, Hyderabad, India, September 2010.

[27] G. Strang and G. Fix. A Fourier analysis of the finite element variational method. *Construct. Asp. Funct.Anal.*, pages 796–830, 1971.

[28] V. A. Zheludev, V. N. Malozemov and A. B. Pevnyi. Filter banks and frames in the discrete periodic case. *Proceedings of the St. Petersburg Mathematical Society, **14**, (2008), AMS Translations, Ser. 2*, 228:1–12, 2009.

[29] V. A. Zheludev. Local spline approximation on a uniform grid. *U.S.S.R. Comput. Math. & Math. Phys.*, 27(5):8–19, 1987.

[30] V. A. Zheludev. Periodic splines and the fast Fourier transform. *Comput. Math. & Math Phys.*, 32:149–165, 1991.